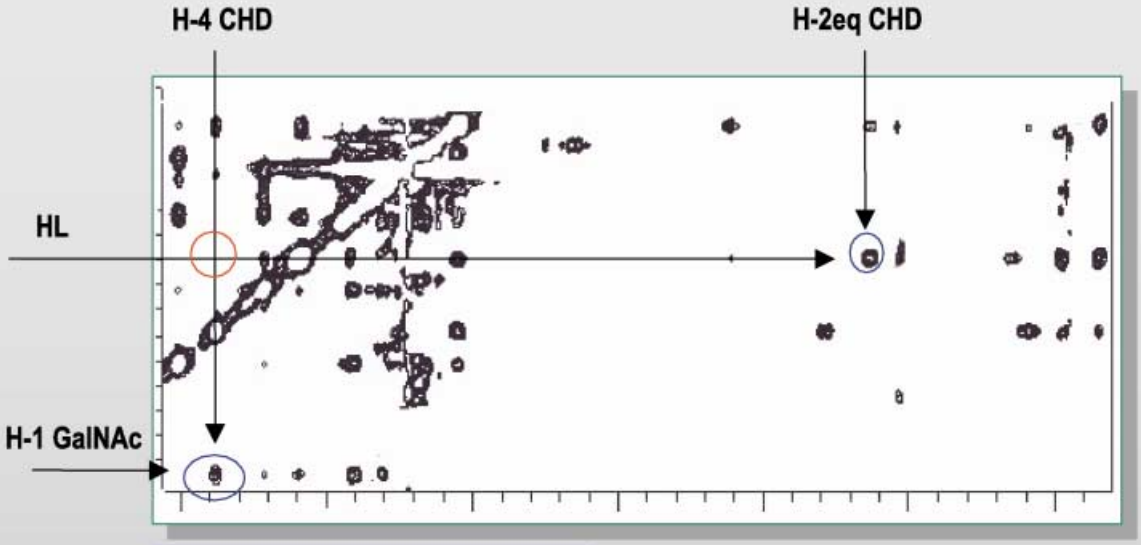

CT:3 complex. Selected region of the TR-NOESY spectrum

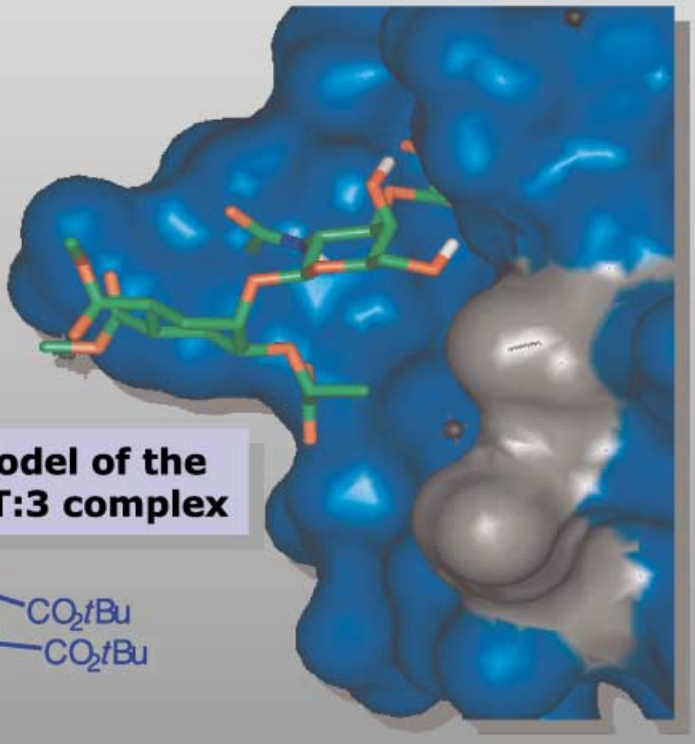

Model of the CT:3 complex

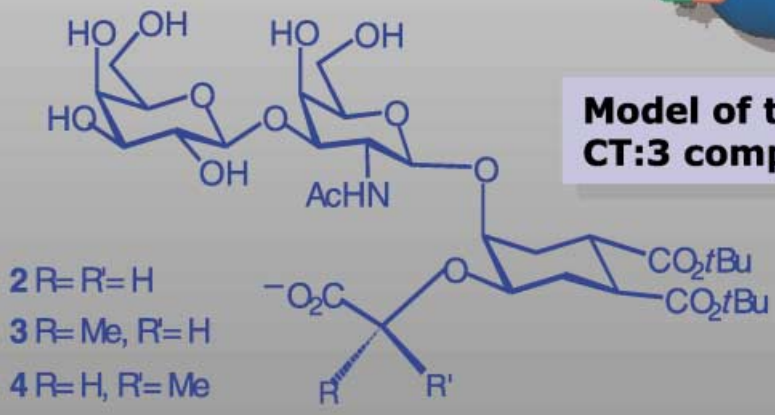

2 R= R'= H
3 R= Me, R'= H
4 R= H, R'= Me

The interaction of ganglioside GM1 mimics 2–4 with the Cholera Toxin has been studied by using NMR spectroscopy and molecular modelling

For more information see the following pages . . .

 © 2002 WILEY-VCH Verlag GmbH & Co. KGaA, Weinheim 0947-6539/02/0820-4597 $ 20.00+.50/0

Second-Generation Mimics of Ganglioside GM1 Oligosaccharide: A Three-Dimensional View of Their Interactions with Bacterial Enterotoxins by NMR and Computational Methods

Anna Bernardi,*[a] Donatella Potenza,[a] Anna Maria Capelli,[b] Alicia García-Herrero,[c] F. Javier Cañada,[c] and Jesús Jiménez-Barbero*[c]

Abstract: As a step to delineate a strategy of ligand design for cholera toxin (CT), NMR studies were performed on several mimics of the GM1 ganglioside oligosaccharide. The conformation of these analogues was investigated first in solution and then upon binding to cholera toxin by transferred nuclear Overhauser effect (TR-NOE) measurements. It was demonstrated that CT selects a conformation similar to the global minima of the free saccharides from the ensemble of presented conformations. No evidence of major conformational distortions was obtained, but one or two of the available conformers of the hydroxyacid side chain appear to be selected in the bound state. The NMR data were interpreted with the aid of computer models, generated and analyzed by using a combination of different approaches (MacroModels' MC/EM and MC/SD, Autodock, and GRID). Analysis of the NMR data supported by computational studies allowed us to interpret the experimental observations and to derive workable models of the ligand:toxin complexes. These models suggest that the higher affinity of the (*R*)-lactic acid derivative **3** may stem from lipophilic interactions with a hydrophobic area in the toxin binding site located in the vicinity of the sialic acid side chain binding region of the CT:GM1 complex, and formed by the side chain of Ile-58 and Lys-34. Thus, the models obtained have allowed us to make useful design suggestions for the improvement of ligand affinity.

Keywords: carbohydrates · carbohydrate–protein interactions · cholera toxin · glycomimetics · NMR spectroscopy

Introduction

The inhibition of protein–carbohydrate interaction provides a powerful strategy for the treatment of a variety of diseases. The development of small-molecule mimics of oligosaccharides capable of inhibiting sugar-binding proteins (lectins) is attracting a great deal of attention as a way to develop drugs with good stability and synthetic availability.[1] Specific binding between bacterial enterotoxins and oligosaccharide receptors on the host cell membrane is a paradigm for protein–sugar interaction. A particularly well-studied system is the recognition pair composed of ganglioside GM1 and the two bacterial enterotoxins, cholera toxin (CT) and the heat-labile toxin of *E. coli* (LT), which use the GM1 headgroup pentasaccharide (o-GM1) as their molecular target to attack and penetrate the host cells. Recently, we described the pseudo-oligosaccharide **1**,[2, 3] a functional and structural mimic of o-GM1 in which the reducing end of the pentasaccharide has been replaced by a conformationally restricted cyclohexanediol (CHD) (Scheme 1).

More recently, we have reported the series of second-generation mimics **2**–**4**,[4] in which the sialic acid (NeuAc) moiety of **1** is also replaced with simpler α-hydroxyacids. Replacement of the NeuAc residue with simplified chemical entities was devised to increase the synthetic accessibility of the artificial receptors, while preserving the acid function of NeuAc, which was shown to be essential for GM1 binding to CT.[5, 6] Indeed, the X-ray structure of the CT:o-GM1 complex[5] reveals that the oligosaccharide binds with a two-fingered grip by using a relatively deeper galactose-binding

[a] Prof. A. Bernardi, Dr. D. Potenza
Dipartimento di Chimica Organica e Industriale
Universita' di Milano, and Centro di Eccellenza CISI
via Venezian 21, 20133 Milano (Italy)
Fax: (+39) 02-50314072
E-mail: anna.bernardi@unimi.it

[b] Dr. A. M. Capelli
GlaxoSmithKline, Medicines Research Centre
-via Fleming 4, 37135 Verona (Italy)

[c] Dr. J. Jiménez-Barbero, Dr. A. García-Herrero, Dr. F. J. Cañada
Dept. of Química Orgánica Biológica
Centro de Investigaciones Biologicas, CSIC, Velazquez 144,
28006 Madrid (Spain)
Fax: (+34) 91-5644853
E-mail: iqoj101@iqog.csic.es

Supporting information for this article is available on the WWW under http://www.chemeurj.org/ or from the author.

 © 2002 WILEY-VCH Verlag GmbH & Co. KGaA, Weinheim 0947-6539/02/0820-4598 $ 20.00+.50/0 *Chem. Eur. J.* **2002**, *8*, No. 20

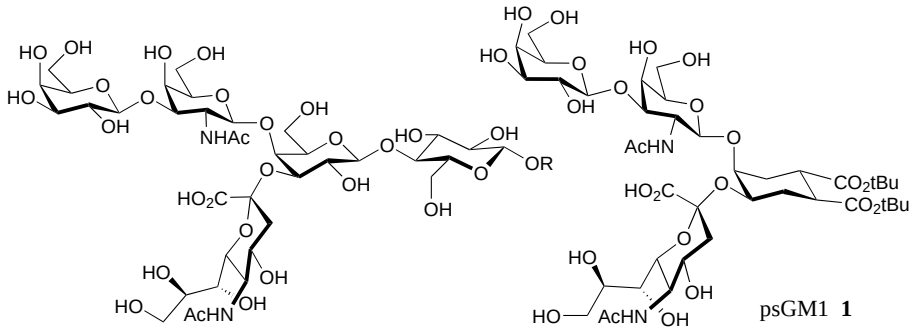

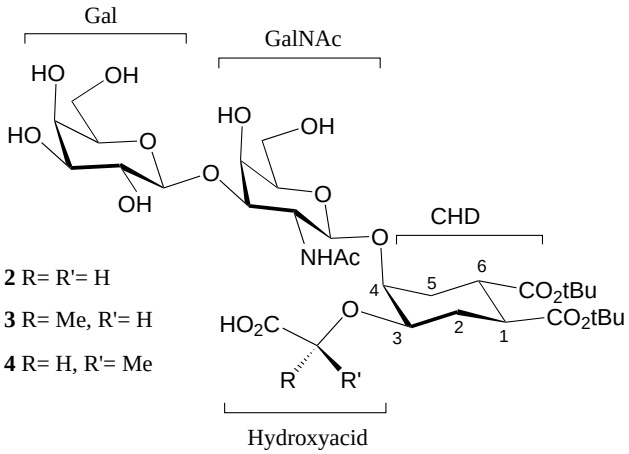

Scheme 1. Mimics of ganglioside GM1 oligosaccharide. Gal: galactose; GalNAc: *N*-acetyl galactosamine; CHD: cyclohexanediol.

pocket and a shallower carboxylate-binding region on the toxin surface. The pseudo-GM1 mimic **1** (psGM1), which preserves the solution conformation of o-GM1,[3] is probably bound in the same orientation. Conformational analysis of **2**–**4** (vide infra) reveals that although the (*R*)-lactic acid derivative **3** and glycolic acid derivative **2** are more flexible than **1**, these should be able to simultaneously fit the galactose- and the carboxy-binding sites of CT by using low-energy conformations. The three ligands were synthesized and their interaction with the cholera toxin B5 pentamer (CTB) was studied by using the intrinsic fluorescence of the Trp-88 residue in the toxin binding site.[7] The dissociation constants determined by nonlinear regression analysis were found to be 667 μM for **2**, 190 μM for **3**, and 1.1 mM for **4**.[4] Thus, the (*R*)-lactic acid derivative **3** displayed the strongest affinity for CTB. For comparison, CTB has a K_D of about 40 mM and 81 mM for galactose and lactose,[7] respectively, and asialoGM1 (GM1 without sialic acid) had no detectable binding to CT at concentrations that were 320 times higher than the IC_{50} of GM1.[6] Thus, the carboxy group of **3** and to a lesser extent of **2**, appears to have a sizeable effect on the affinity of the artificial receptors for CT.

Since ligand binding of cholera toxin appears to primarily engage the nonreducing Gal moiety,[5] it is an intriguing quest to comparatively delineate the bound-state topologies of the studied ligands. Information about the conformation of complexed ligands can be derived from transferred nuclear Overhauser effect (TR-NOE) studies[8] provided that the exchange between the complexed and uncomplexed states is sufficiently fast.[9, 10] Application of this methodology allows one to study how the ligand fits into a protein binding site in solution. Overall, it is fair to say that the conditions required to monitor TR-NOEs have so far appeared to be frequently satisfied by sugar receptors.[11]

Herein we report a detailed computational and NMR study of o-GM1 mimics **2**–**4** and of their complexes with bacterial enterotoxins CT and LT. By building on conformational studies with these free ligands in solution, we will be able to determine whether a low-energy conformer is selected and which one, or whether the binding process entails a linkage distortion. We unequivocally demonstrate that only *syn* conformations[12] around the glycosidic linkages of these analogues are recognized by CT, and that the toxin selects a preferred orientation of the lactic/glycolic side chain, probably through the establishment of key hydrogen bonds with the water molecule at crystallographic site 3[5] and with the backbone NH of the aminoacid 13 of the toxin (Arg-13 in LT, Hys-13 in CT). The model strongly suggests that the lipophilic interaction of the (*R*)-lactic acid side chain of **3** with a hydrophobic patch in the toxin binding pocket may be the origin of the highest affinity of this ligand in the series studied here.

Definitions: Residues of the pseudo-sugars **2**–**4** are defined as indicated in Scheme 1. The CHD residue is numbered as depicted in Scheme 1 to facilitate comparison with the branching galactose unit of GM1.

Glycosidic angles are defined as follows: Galβ1-3GalNAc: ϕ = GalH1-GalC1-O1-GalNAcC3, ψ = GalC1-O1-GalNAcC3-GalNAcH3; for Galβ1-4CHD: ϕ = GalH1-GalC1-O1-CHDC4, ψ = GalC1-O1-CHDC4-CHDH4; hydroxyacid-CHD: ϕ = C(=O)-C_α-O-CHDC3, ψ = C_α-O-CHDC3-CHDH3, χ = C(=O)-C_α-CHDC3-CHDH3.

Results

The free state: NMR studies: The relationship between NOEs and proton–proton distances is well established[13] and can be

worked out, at least semiquantitatively, when a relaxation matrix analysis is considered. The NOE intensities reflect the conformer populations, and therefore information on the population distributions in free solution can be obtained by focusing on these key NOEs.[14] The assignment of the ^{1}H and ^{13}C NMR resonances of the three molecules was performed by using standard two-dimensional experiments, COSY, TOCSY, and HSQC (see Supporting Information). Then, selective one-dimensional NOESY and two-dimensional T-ROESY experiments were performed on **2**–**4** to provide experimental distances and to derive the average conformation or conformational equilibria present in solution. Oligosaccharide conformations are defined by the corresponding torsion angles around the glycosidic linkages and by the torsions around the hydroxyacid side chains. In principle and as is usually found in oligosaccharides, there are exclusive NOEs that unequivocally characterize the three preferred regions of the potential energy surfaces of beta-linked disaccharides: *syn*ϕ-*syn*ψ, *syn*ϕ-*anti*ψ, and *anti*ϕ-*syn*ψ (Figure 1).[15, 16] The

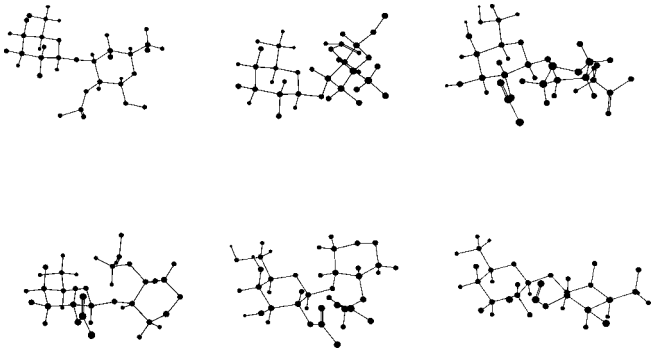

Figure 1. Schematic view of the three major orientations around the glycosidic linkages of the disaccharide and pseudo-disaccharide fragments of glycomimetics **2**–**4**. The Galβ(1→3)GalNAc linkage (top), the GalNAcβ(1→4)CHD linkage (bottom), and from left to right, the *syn*ϕ-*syn*ψ, *anti*ϕ-*syn*ψ, and *syn*ϕ-*anti*ψ conformers, respectively.

analysis of the vicinal proton–proton coupling constants for the six-membered rings indicated that the Gal and GalNAc chairs are in the $^4C_1$ conformation, while the CHD also adopts a chair conformation with the bulky *tert*-butoxycarbonyl groups in equatorial orientations. Vicinal $J_{5,6}$ couplings for the hydroxymethyl groups were also extracted. The coupling values were 7–8 Hz for both the Gal and GalNAc entities in all the compounds, in agreement with a *gt*:*tg* equilibrium of the ω torsion angle, as is usually the case for galactose moieties.[17]

The orientation around the Galβ(1→3)GalNAc linkage should be defined by the NOEs between H1 Gal and the protons on the aglyconic GalNAc moiety, especially H3, H4, and H2. In fact, the Gal-H1/GalNAc-H3 cross peak is always very strong (for the three compounds), indeed even stronger than the corresponding Gal-H1/Gal-H3 and Gal-H1/Gal-H5 intraresidue cross peaks (Figure 2). A very weak Gal-H1/GalNAc-H4 and an even weaker Gal-H1/GalNAc-H2 cross peak are also detected, although the latter is just above the noise level and not seen in Figure 2. According to relaxation matrix calculations, the Gal-H1/GalNAc-H3 distance should

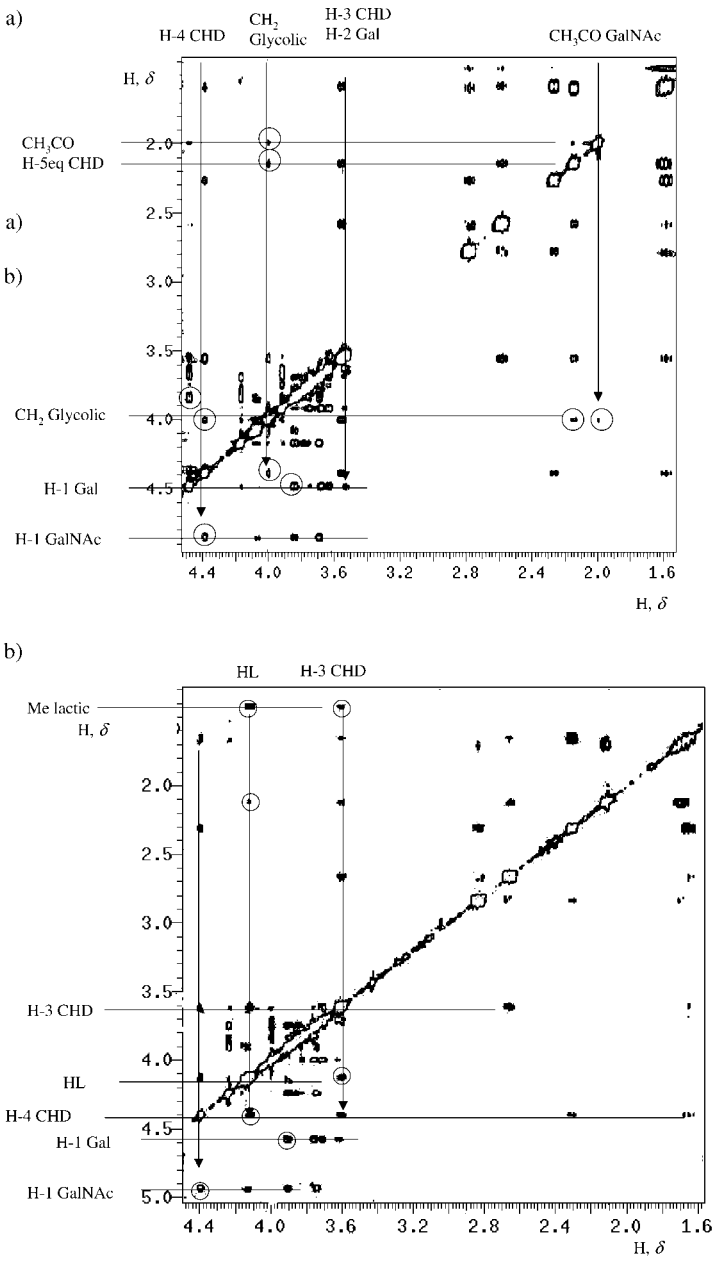

Figure 2. Key region of the 500 MHz ^{1}H NMR NOESY spectrum recorded for a) **2** and b) **4**. Relevant interresidue cross peaks are indicated.

be 2.4 ± 0.1 Å, while Gal-H1/GalNAc-H4 is 3.5 ± 0.2 Å. The Gal-H1/GalNAc-H2 is longer than 3.6 Å. Therefore, these distances can be correlated for all three compounds with one major orientation around the Galβ(1→3)GalNAc ϕ/ψ torsion angles. This region corresponds to the global minimum *syn* conformation, which is characterized by ϕ,ψ of around 55°,0°.

A similar situation occurs for the GalNAcβ(1→4)CHD moiety, with the same NOE pattern. In fact, only the very strong interresidue GalNAc-H1/CHD-H4 cross peak is observed. The corresponding GalNAc-H1/CHD-H5ax, GalNAc-H1/CHD-H5eq, and GalNAc-H1/CHD-H3 are below the noise level. The observed cross peak corresponds to a GalNAc-H1/CHD-H4 distance of 2.4 ± 0.1 Å, while those between GalNAc-H1 and CHD-H5ax, CHD-H5eq, and

© 2002 WILEY-VCH Verlag GmbH & Co. KGaA, Weinheim
0947-6539/02/0820-4600 $ 20.00+.50/0 *Chem. Eur. J.* **2002**, *8*, No. 20

CHD-H3 are probably longer than 3.5 Å. Again, the average conformation in solution for this linkage corresponds to the global minimum *syn* conformer characterized by $\phi,\psi = 30°,30°$. The existence of conformers in the *anti*-ϕ or *anti*-ψ regions with populations above 5% can be neglected, since otherwise their exclusive NOEs would have been observed. Regarding the orientation of the acetamide moiety, in all the three cases the cross peak of the methyl group with the corresponding GalNAc-H2 has a weak intensity, while no cross peaks to either GalNAc-H1 or GalNAc-H3 are observed. Therefore, the major orientation in solution is that with the methyl group pointing out of the pyranose ring, with an *anti*-like relationship to C-2.

Table 1. Experimental and calculated distances for the hydroxyacid fragment of free **2**–**4**.

Ligand	Contact	Exp. distance [Å]	Calcd Distance [Å] (AMBER*, MC/EM)[a]	Calcd distance [Å] (Kolb, MC/SD)[b]
2	CH_2/CHD-H4	2.6–2.8	3.0[c]	3.2[c]
	CH_2/CHD-H3	2.4–2.6	2.6[c]	2.6[c]
	CH_2/CHD-H2eq	2.6–3.0	3.6[c]	3.0[c]
	CH_2/GalNAc-H1	2.7–3.3	3.1[c]	3.0[c]
	CH_2/GalNAc-Me	2.9–3.1	5.0	4.3
3	HL/CHD-H4	2.4–2.6	2.6	2.6
	HL/CHD-H3	2.4–2.6	2.6	2.4
	HL/CHD-H2eq	2.6–3.0	3.5	3.6
	HL/GalNAc-H1	2.8–3.2	2.7	2.9
	MeL/GalNAc-H1	2.8–3.4	3.4	2.9
	MeL/CHD-H3	2.9–3.3	3.9	3.8
	MeL/CHD-H4	>3.5	4.0	4.2
	MeL/CHD-H2eq	>3.5	4.4	4.2
4	HL/CHD-H4	2.4–2.6	3.8	3.8
	HL/CHD-H3	2.4–2.6	2.4	2.4
	HL/CHD-H2eq	2.8–3.2	3.1	2.5
	HL/GalNAc-H1	2.9–3.5	4.1	4.2
	MeL/GalNAc-H1	>3.5	4.0	4.0
	MeL/CHD-H3	2.5–2.9	4.3	4.0
	MeL/CHD-H4	2.9–3.5	5.0	5.0
	MeL/CHD-H2eq	>3.5	4.7	4.0

[a] Distances are calculated as $< r^{-6} >^{-1/6}$, in which $< r^{-6} >$ is the Boltzmann average of the r_i^{-6} of the individual conformations within 12 kJ mol^{-1} of the global minimum. [b] Calculated from $< r^{-6} >$ monitored during the simulation (MDDI option of Batchmin). [c] Average over the two protons (CH_2 is isochronous).

Additional torsional degrees of freedom are available for these molecules, which correspond to the hydroxyacid side chains. The two rotatable bonds here are not restricted by anomeric or *exo*-anomeric effects, and may assume a broader range of orientations. In principle, three idealized staggered orientations may be defined (Figure 3), although rotations around the O–C bond may also produce quasi-eclipsed orientations. The major orientation around the lactic acid-containing derivatives can be defined by focusing on the NOEs from the CH (HL) and CH_3 groups of this moiety to H-3, H-4, H-2eq, H-2ax of CHD, and to H-1 and the acetamide methyl group of GalNAc (Table 1). Thus, the NOE patterns for the side chain substituents of the acid are best examined in terms of the three staggered orientations of Figure 3 and correlated to the improper dihedral angle χ C(OOH)-C_α-C3-H3.

For the *R* isomer **3**, the NOE intensity of the HL/CHD-H4 cross peak is higher than that of the HL/CHD-H2eq cross peak and is similar to that for the vicinal HL/CHD-H3. The HL/GalNAc-H1 displays a peak of medium-weak intensity, and no HL/CHD-H2ax peak is detected. The corresponding distances are 2.5 ± 0.1 (to CHD-H4 and to CHD-H3), 2.8 ± 0.2 (CHD-H2eq), 3.0 ± 0.2 (GalNAc-H1), and more than 3.5 Å (HL/CHD-H2ax), respectively (Table 1). In turn, the CH_3 methyl of the (*R*)-lactic side chain only displays weak cross peaks to its vicinal CHD-H3 (3.1 ± 0.2 Å) and to GalNAc-H1 (3.1 ± 0.3 Å). No cross peaks are observed between the methyl group and CHD-H2eq or CHD-H4.

These results are in agreement with a major $\chi = +60°$ conformer (with an *anti*-type relationship between the methyl group and the CHD-H3, Figure 3), although the $\chi = 180°$ rotamer (displaying the carboxyl group *anti* to CHD-H3) must also be contributing to the conformational equilibrium to account for the HL/CHD-H2eq distance. A nonidealized staggered conformation of the former type may also satisfactorily explain the observed NOE pattern.

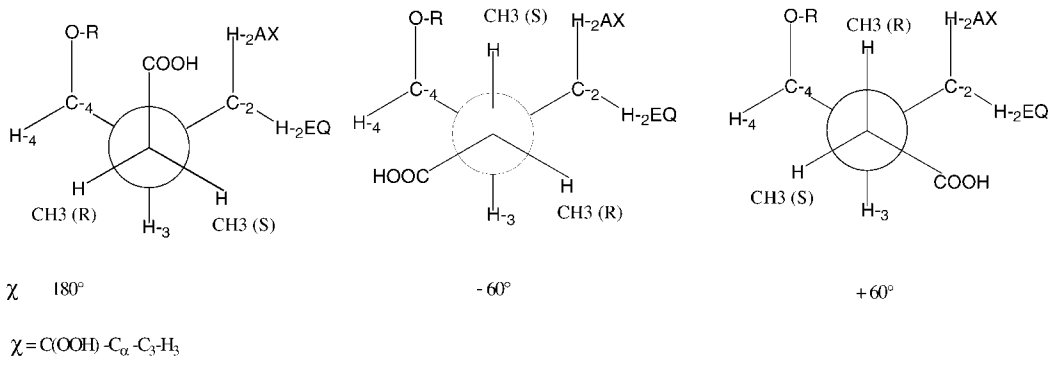

Figure 3. Schematic view of the three idealized staggered orientations of the hydroxyacid chains with respect to the CHD moiety. Deviations from the idealized 60° orientations may take place. The improper dihedral angle χC(OOH)–C_α–C_3–H_3 defines the orientation of the carboxy group relative to the cyclohexyl ring.

 © 2002 WILEY-VCH Verlag GmbH & Co. KGaA, Weinheim 0947-6539/02/0820-4601 $ 20.00+.50/0

For the *S* analogue **4**, the NOE intensity of the vicinal HL/CHD-H3 cross peak is also similar to that of the HL/CHD-H4 connectivity. Very weak cross peaks are observed for the HL/GalNAc-H1 and HL/CHD-H2eq connectivities, and no HL/CHD-H2ax peak is detected. The intensities correspond to interproton distances of 2.5 ± 0.1 (to CHD-H3 and to CHD-H4), 3.0 ± 0.2 (CHD-H2eq), and 3.1 ± 0.3 Å (GalNAc-H1). In addition, the CH_3 methyl of the (*S*)-lactic side chain has a medium intensity cross peak to its vicinal CHD-H3 proton (2.7 ± 0.2 Å), which is slightly weaker than that to its geminal HL (Figure 2b). A weak cross peak to CHD-H2eq is also present (3.1 ± 0.3 Å). No cross peak to GalNAc-H1 is observed.

This NOE pattern agrees with a major $\chi = 180^\circ$ conformation (*anti*-type relationship between the COOH group and the CHD-H3, Figure 3), although the $\chi = -60^\circ$ rotamer (displaying the methyl group *anti* to CHD-H3) also probably contributes to the conformational equilibrium. Alternatively, a nonidealized staggered $\chi = +180^\circ$ conformation with closer proximity between HL and CHD-H4 may also satisfactorily explain the observed NOEs.

In the glycolic compound **2**, the two CH_2 protons are isochronous. Thus, no distinction may be made between the individual *pro-S* and *pro-R* protons. Their NOE cross peaks with H-3 and H-4 of the CHD moiety display similar intensities, which are in turn somewhat higher than that with CHD-H2 eq. The corresponding interproton distances are 2.5 ± 0.1 (CHD-H3), 2.7 ± 0.1 (CHD-H4), and 2.8 ± 0.2 Å (CHD-H2eq), respectively. Weak cross peaks between the CH_2 and GalNAc-H1 and between the CH_2 and methyl acetamide GalNAc should correspond to average distances of 3.0 ± 0.3 Å. The CH_2/CHD-H2ax should again be longer than 3.5 Å (Figure 2a).

A conformational equilibrium between $\chi = +180^\circ$ and $\chi = +60^\circ$ (Figure 3) can satisfactorily describe the observed NOEs. Again and alternatively, a nonidealized staggered orientation of the COOH *anti* to CHD-H3 conformation with closer proximity between one of the CH_2 protons and the CHD-H4 may also satisfactorily explain the observed NOE pattern.

Conformational analysis of free ligands 2–4: The conformation of the free ligands was extensively investigated by using MacroModel (MMOD). Two sets of parameters were employed in the MC/EM searches for the hydroxyacid fragment: the original AMBER* parameters, and those explicitly developed for hydroxyacids by Kolb and Ernst.[18] The latter were also used in the MC/SD simulations of the free ligands in GB/SA water solution. The protocols employed had been previously validated for o-GM1 and other ganglioside headgroups by comparison with NMR data.[19] The calculations revealed that the Gal-GalNAc-CHD fragment of all three molecules populated the *syn* conformation for both glycosidic linkages in agreement with the experimental data discussed above. Minima were located at $\phi,\psi = 50^\circ,0^\circ$ for the Gal–GalNAc linkage and $25^\circ,30^\circ$ for the GalNAc–CHD linkage. Some flexibility around this area (but not outside) was shown in the dynamic simulations ($\phi,\psi = 50^\circ \pm 20^\circ, 0^\circ \pm 30^\circ$ for Gal-GalNAc and $40^\circ \pm 30^\circ, 25^\circ \pm 25^\circ$ for GalNAc-CHD) The predicted interglycosidic distances are very short (2.2–2.4 Å) for the Gal-H1/GalNAc-H3 and GalNAc-H1/CHD-H4 pair, whereas much longer distances were calculated for Gal-H1/GalNAc-H2 (4.1–4.2 Å), Gal-H1/GalNAc-H4 (3.6–3.9 Å). These predictions are similar to what was calculated for other gangliosides and for psGM1,[3, 19] and are confirmed by the NMR experiments on **2–4**, which are consistent with a *syn* population $\geq 95\%$ for all three molecules.

The computational description of the hydroxyacid side chain is only qualitatively correct, as judged by comparison with the NOE data. The calculated and experimental distances for this fragment are reported in Table 1. All calculations, and particularly those using Kolb's parameters, predict a limited flexibility for the side chain, and a large preference for the methyl group or one of the glycolic acid hydrogens to be antiperiplanar relative to the CHD-C3 (χ *gauche* conformations in Figure 3). Although NMR results indicate that these rotamers do indeed appear to be populated, the NOE results for all molecules have a set of comparable NOESY cross peaks from the hydroxyacid HL proton to CHD-H3 and CHD-H4, accompanied by weaker interactions with CHD-H2eq. This is consistent with a higher flexibility for the hydroxyacid fragment than calculated. Moreover, the NMR results for the glycolic acid derivative **2** and the (*S*)-lactic acid derivative **4** are consistent with a major χ *anti* conformer, which is not found at low energy by the calculations (see Table 4). A better agreement is achieved for the *R* derivative **3**, which is calculated to be a mixture of $\chi = +60^\circ$ and $\chi = 180^\circ$ conformations, that is, the same two conformations supported by experiment. As a result, the calculated HL/CHD-H4 distance for **3** is comparable to the NMR value (Table 1), and the calculated HL/CHD-H2eq distance is somewhat longer than supported by experiment (Table 1). In general, comparison with the experimental results (see Table 4) reveals that in reality the $\chi = 180^\circ$ conformation is more heavily populated than expected by either force field calculations. Since the performance of the Kolb's force field is superior to AMBER*'s for the *R* derivative **3**, which is the best binder of the series, the Kolb's parameters were used for all subsequent calculations.

The bound state: NMR studies: The addition of the cholera toxin CTB pentamer to a D_2O solution of **2–4** induced broadening of resonance signals of the glycomimetic protons, especially those belonging to the Gal moiety (Figure 4). Those for the GalNAc units were also broadened, although to a lesser extent, with the exception of GalNAc-H4, which also displayed important broadening. This change in a signal parameter is a clear indication of binding and therefore enabled further study.

First, saturation transfer difference (STD) experiments were performed. In STD experiments[20, 21] the host protein is irradiated, and the saturation transfer to the ligand gives rise to signal enhancements that are stronger for the protons in closest proximity with the protein. Thus, STD experiments can be used to identify the epitope of the glycomimetics. Typical results are illustrated by the STD spectrum of the CT:**2** complex (Figure 5). Indeed, the strongest glycomimetic signals that appeared upon irradiation of the protein envelope corresponded to the Gal protons along with H2, H4, and the

 © 2002 WILEY-VCH Verlag GmbH & Co. KGaA, Weinheim 0947-6539/02/0820-4602 $ 20.00+.50/0 *Chem. Eur. J.* **2002**, *8*, No. 20

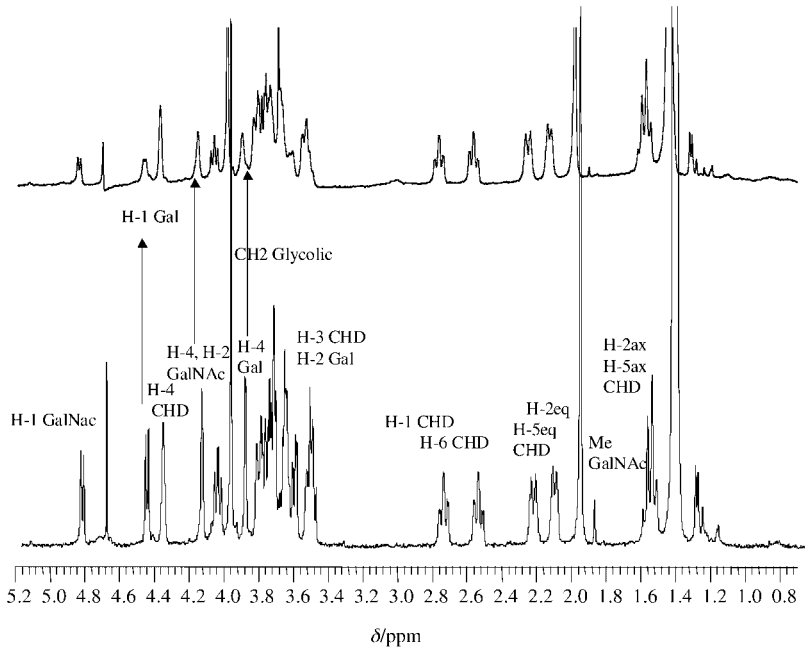

Figure 4. Bottom: ^{1}H NMR spectrum of compound **2**. Top: ^{1}H NMR spectrum of **2** upon addition of CTB (molar ratio 25:1). The major linewidth variations are observed for the Gal protons, followed by the GalNAc signals. Minor differences are observed for the protons belonging to the CHD moiety. Some background signals of the toxin are also observed.

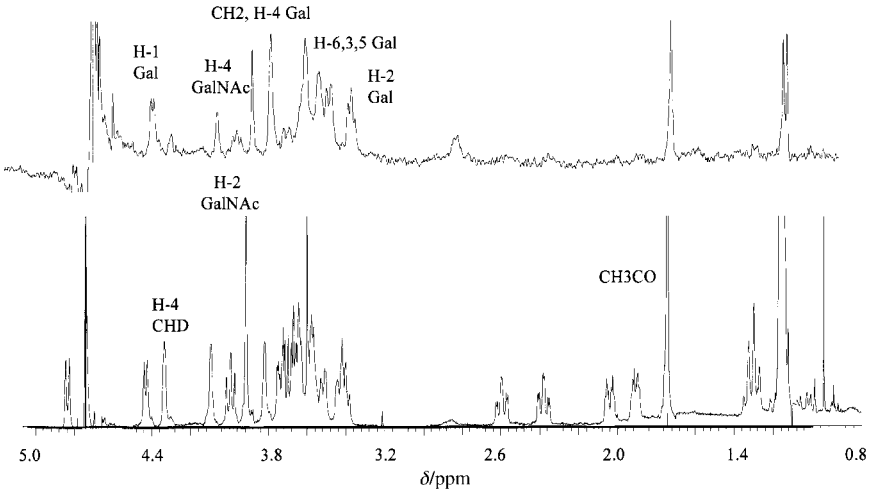

Figure 5. Bottom: ^{1}H NMR spectrum of compound **2** upon addition of CTB (molar ratio 25:1). Top: STD spectrum (off-resonance saturation minus on-resonance saturation at the protein aromatic region) for compound **2** upon addition of CTB (molar ratio 25:1). The Gal protons and some GalNAc protons (with minor intensities) are observed. No signals are observed for the protons belonging to the CHD moiety, while the hydroxyacid CH_2 is also evident.

acetamide methyl group of GalNAc. Small intensities corresponding to GalNAc-H3 and the glycolic CH_2 side chain were also evident. The other protons of GalNAc and the cyclohexane moiety were less evident, which indicated that the key mimetic/toxin contacts take place through the nonreducing Gal unit. Contacts with the GalNAc moiety in the vicinity of the attachment point of the Gal residue and on the sialic acid surrogate (hydroxyacid) also take place.

Next, one-dimensional and two-dimensional TR-NOESY experiments (Figure 6) were performed to deduce the bound conformation of **2**–**4**. Different mixing times and protein/ligand molar ratios were systematically tested towards this end. This experiment provides an adequate tool to determine the conformation of the bound ligand for those ligands that exchange rapidly with the free state. In complexes of large molecules, cross-relaxation rates of the bound compound are opposite in sign to those of the free ligand, and generate negative NOEs. Indeed, TR-NOESY experiments (Figures 6a and 6b) produced strong and negative NOEs, as expected for ligand binding. These signals are the basis for assignment of the conformational properties of the bound state. In all cases, the strongest interglycosidic peaks in the spectra can be attributed to the recognition of *syn*-ϕ,ψ conformers for both glycosidic linkages. For the GalNAcβ(1→4)CHD and Galβ-(1→3)GalNAc glycosidic linkages of the three compounds, the same pattern of inter and intraresidue NOEs was observed, with strong GalNAc-H1/CHD-H4 and Gal-H1/GalNAc-H3 cross peaks, indicating bound-state distances around 2.3–2.5 Å. A very weak Gal-H/GalNAc-H4 cross peak, corresponding to a 3.6 Å interproton distance is also observed. No other interresidue contacts are observable. T-ROESY experiments allowed us to exclude spin-diffusion effects for the key cross peaks. Fittingly, the abovementioned cross peaks had a different sign relative to the diagonal peaks, thus excluding the possibility of protein-relayed or spin-diffusion-mediated correlations. The use of a full matrix relaxation approach, including exchange between the free and bound forms, is instrumental to estimate the expected NOEs for the binding of other possible *anti*-ψ and *anti*-ϕ families. Thus, TR-NOE calculations for individual *anti* and *syn* conformers were performed and compared to the experimental data. No evidence for the recognition of the *anti* conformations could be found for the Gal–GalNAc and GalNAc–CHD linkages. Indeed, the very short Gal-H1/GalNAc-H2 (2.3 Å) and Gal-H2/GalNAc-H3 (2.3 Å) distances for the corresponding *anti*-ψ and *anti*-ϕ conformations would give rise to detectable TR-NOE cross peaks (above 1% intensity of the diagonal peak), if populated above 5–10%.

 © 2002 WILEY-VCH Verlag GmbH & Co. KGaA, Weinheim 0947-6539/02/0820-4603 $ 20.00+.50/0

An analogous reasoning may be used to elucidate the conformation of the GalNAc–CHD linkage. No NOEs from GalNAc-H1 to H5 or H3 of the cyclohexyl moiety are observable (see, for instance Figure 6b). Thus, the full matrix relaxation calculations allow us to conclude that the presence of the *anti-*ψ and *anti-*ϕ families above a 5–10% of population density can definitely be excluded. As observed in the free state, in all cases the cross peak intensities of the acetamide methyl group and the GalNAc-H2 are weak, indicating an *anti*-like relationship between the GalNAc-C2 and the acetamide CH_3.

Thus, no difference is observed between the free-state and bound-state conformations of the Gal-GalNAc and GalNAc-CHD fragments: also in the CT binding pocket, **2**–**4** populate the so-called *syn* conformation (ϕ,ψ 55°,0°) of both glycosidic linkages.

In contrast, clear differences in cross peak intensities of bound and free state were observed for the NOEs involving the hydroxyacid side chain protons (HL, or CH_2 for **2**, and CH_3). The largest variations occur for **2** and **3**. In the (*R*)-lactic (**3**) and glycolic (**2**) compounds, the intensity of the HL (or CH_2 for **2**) cross peak with CHD-H4 is much weaker than that between the HL (or CH_2 for **2**) with CHD-H2eq, which is, opposite to the observations in the free state (Figures 6a–c, Table 2). This intensity change, which corresponds to a torsional variation of the side chains, now places the HL of the (*R*)-lactic chains at about 2.6 ± 0.3 Å average distance from the H2eq of the CHD moiety. The average distance is somewhat smaller for the glycolic derivative: 2.5 ± 0.2 Å. In the *R* derivative **3** (Figure 6b), the cross peak of the HL group with CHD-H3 has a medium intensity, corresponding to a distance of 2.6 ± 0.3 Å (free state: 2.8 ± 0.2 Å; 2.6 ± 0.2 Å for the glycolic derivative; free: 2.8 ± 0.2 Å), while that with CHD-H4 is very weak in both cases (3.4 ± 0.3 Å; free **3**: 2.5 ± 0.1 Å, free **2**: 2.7 ± 0.1 Å). Medium-weak and weak HL/CHD-H2ax cross peaks were also observed for **2** and **3**, respectively (2.9–3.3 Å; not seen in free state). Additionally, for the (*R*)-lactic analogue **3**, the cross peak of the CH_3 group with CHD-H3 has a medium-strong intensity, corresponding to a distance of 2.6 ± 0.3 Å (free: 3.1 ± 0.2 Å), while those with CHD-H2eq (ca. 3.3 Å; free: >3.5 Å) and CHD-H4 (ca. 3.1 Å; free: >3.5 Å) are weak. No connectivities between GalNAc-H1 and either the HL (free: 3.0 ± 0.2 Å) or CH_3 (free: 3.1 ± 0.3 Å) groups of the (*R*)-lactic moiety (CH_2 of the glycolic derivative; free: 3.0 ± 0.3 Å) are observed, and therefore the corresponding interproton distances are larger than 3.4 Å.

Therefore, for the *R* derivative **3** in the bound state, the χ = 180° conformation (with an *anti*-like relationship of the

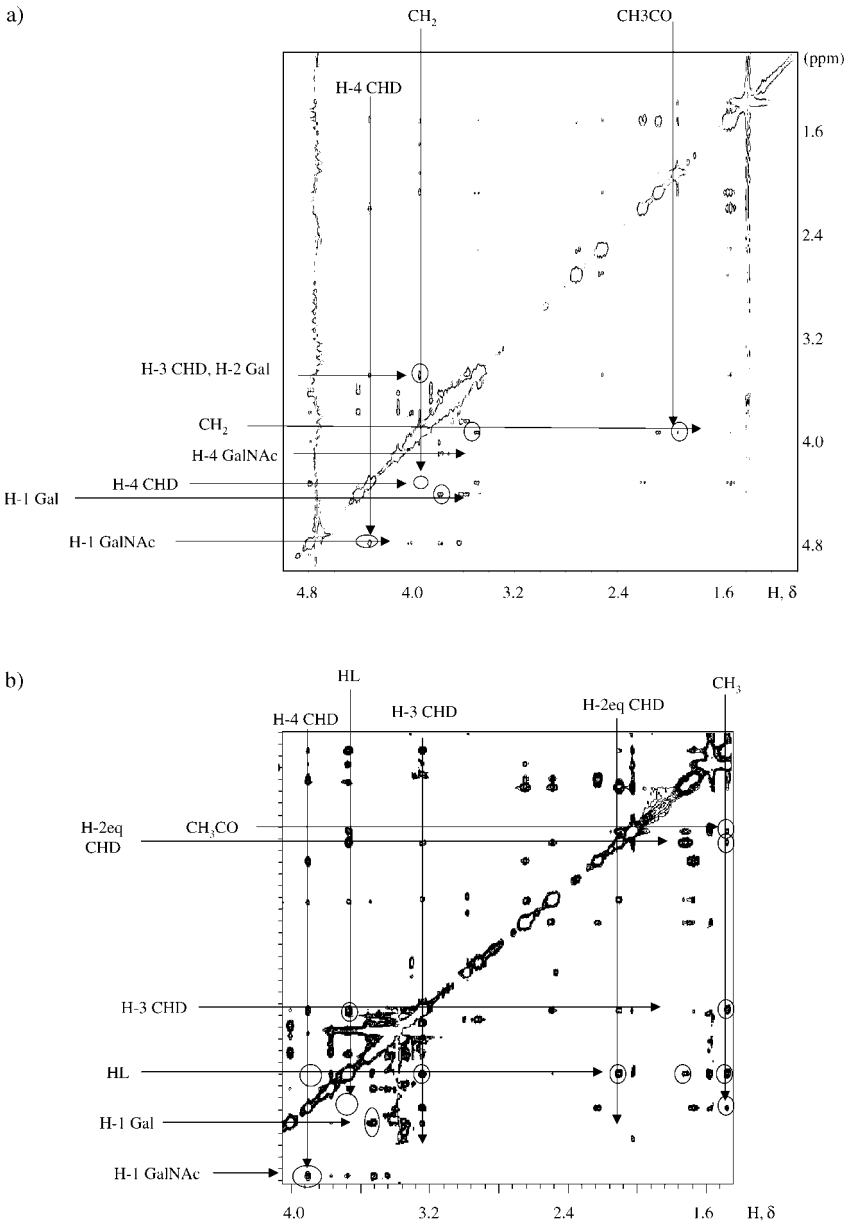

Figure 6. a) 500 MHz ^{1}H NMR NOESY spectrum of the **2**:cholera toxin complex (molar ratio of 35:1, mixing time 200 ms). Relevant interresidue cross peaks are indicated. Additionally, open circles represent cross peaks that were present in the free state and that no longer appear for the bound state (i.e., glycolic CH_2/CHD-H4), indicating a conformational selection process. b) 500 MHz ^{1}H NMR NOESY spectrum of the **3**:cholera toxin complex (molar ratio of 35:1, mixing time 200 ms). Relevant interresidue cross peaks are indicated. Additionally, open circles represent cross peaks that were present in the free state and that no longer appear for the bound state (i.e., HL/CHD-H4), indicating a conformational selection process.

© 2002 WILEY-VCH Verlag GmbH & Co. KGaA, Weinheim
0947-6539/02/0820-4604 $ 20.00+.50/0 *Chem. Eur. J.* **2002**, *8*, No. 20

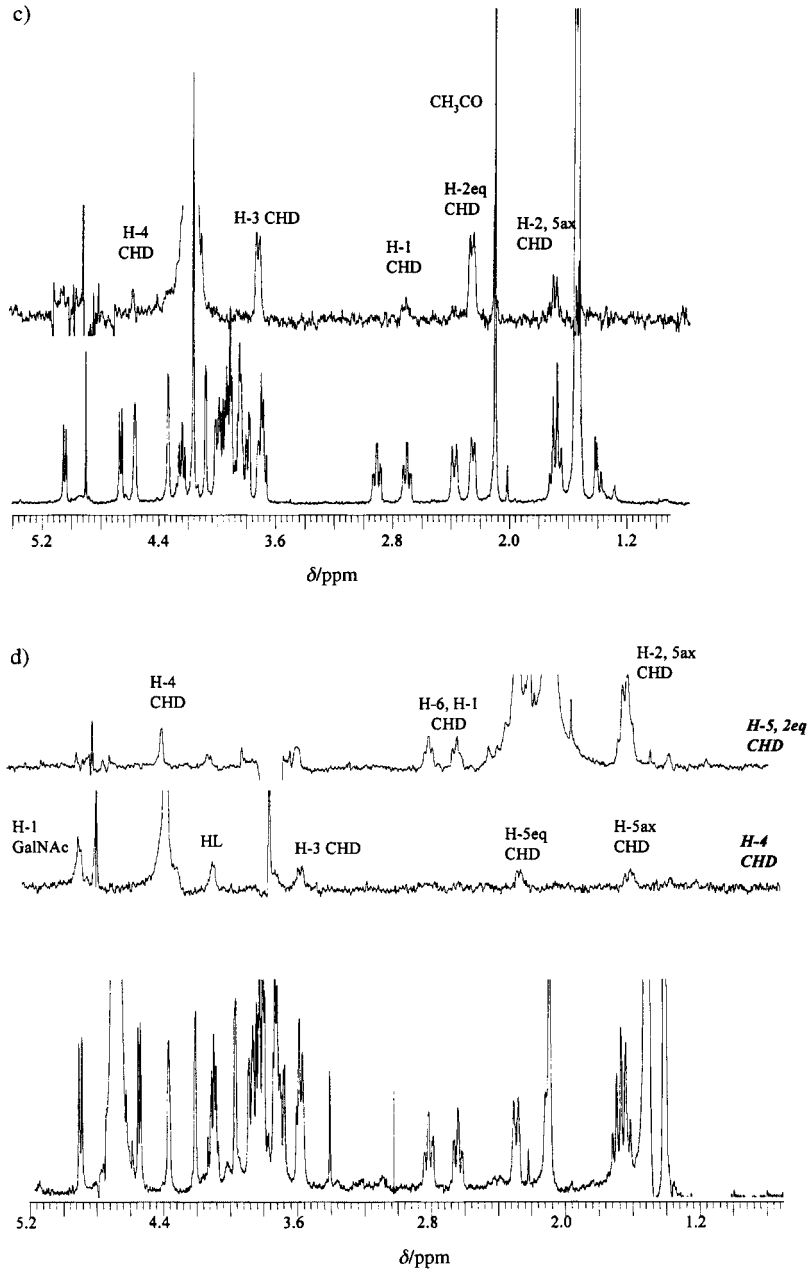

Figure 6. (cont). c) 500 MHz ^{1}H NMR one-dimensional DPFGE-NOESY spectrum of the **2**:cholera toxin complex (molar ratio of 35:1, mixing time 200 ms). Relevant interresidue cross peaks are indicated after selective inversion of the methylene group (CH_2) of the hydroxyacid chain. A strong peak to CHD-H2eq is seen, while only a very weak peak to CHD-H4 is observable in the spectrum, indicating a case of conformational selection. d) 500 MHz ^{1}H NMR one-dimensional DPFGE-NOESY spectrum of the **4**:cholera toxin complex (molar ratio of 35:1, mixing time 200 ms). Relevant interresidue cross peaks are indicated after selective inversion of the CHD-H5eq and CHD-H2eq (top), and CHD-H4 (center).

COOH and CHD-C3, Figure 3) appears to be preferred. The presence of the CH_3/CHD-H2eq and HL/CHD-H2ax cross peaks may also indicate a minor contribution of the $\chi = -60^\circ$ conformer. Hence, the $\chi = 180^\circ$ conformer, which was present as a minor isomer in the free state of **3**, appears to be selected for binding to CT (see Table 4).

For the glycolic derivative **2**, the NOE pattern agrees with a major $\chi = 180^\circ$ conformer (displaying the COOH group *anti* to C3 of the CHD moiety; see Figure 3), although, also in this case, the increase in the HL/CHD-H2 interaction may signal the presence of a $\chi = -60^\circ$ conformation.

In contrast, only minor differences in NOE patterns are observed between free and bound states for the *S* analogue **4**. In the bound state, the HL/CHD-H3, HL/CHD-H4, and HL/CHD-H2eq cross peaks have similar intensities, with distances corresponding to 2.6 ± 0.3 Å (free: 2.5 ± 0.1 Å), 2.7 ± 0.3 Å (free: 2.5 ± 0.1 Å), and 3.0 ± 0.3 Å (free: 3.0 ± 0.2 Å), respectively. In turn, the GalNAc-H1/HL distance is higher than 3.3 Å (free: 3.2 ± 0.3 Å). No connectivities between GalNAc-H1, CHD-H2ax, or CHD-H4 with the CH_3 group of the (*S*)-lactic lateral chain are observed, while the CH_3/CHD-H3 and CH_3/CHD-H2eq connectivities present cross peaks corresponding to distances of approximately 2.8 Å (free: 2.7 ± 0.2 Å) and 3.1 Å (free: >3.5 Å). Thus, little change is observed relative to the free state (see Table 4). These data are in agreement with the appreciable contribution of the two conformations $\chi = 180^\circ$ (major) and $\chi = -60^\circ$ (minor) to the complex description.

Thus, the NMR data suggest that *in all cases a major $\chi = 180^\circ$ conformer is bound to the toxin* (see Table 4). The conformation of the *S* derivative **4** remains essentially unchanged on going from solution to the CT complex. In contrast, CT selects a minor solution conformation ($\chi = 180^\circ$) of the *R* derivative **3**. A conformational change is also suggested for the glyco derivative **2**, although in this case the major $\chi = 180^\circ$ conformer appears to be conserved both in solution and in the complex.

Computational model of the complexes: Docking of **2**–**4** in the LT binding site was attempted by using the MacroModel-based MC/EM protocol that we had validated for o-GM1. However, due to the relatively low affinity of these ligands, they tend to wander out of the binding cavity during the MC steps, so that the Gal-binding site is very poorly fitted. We have already observed this feature working with the lactose-LT complex.[22] Lactose also binds in the LT galactose-binding

Table 2. Experimental and calculated distances for the hydroxyacid fragment of bound **2**–**4**.

Ligand	Contact	Exp. distance [Å]	Calcd distance [Å] Autodock[a]	Calcd distance [Å] MacroModel (MC/SD)[b]
2	CH_2/CHD-H4	> 3.4	3.9,[c] 3.6,[c] 4.2,[c] 4.2[c]	3.4[c]
	CH_2/CHD-H3	2.4–2.8	2.55,[c] 2.5,[c] 2.5,[c] 2.5[c]	2.5[c]
	CH_2/CHD-H2eq	2.3–2.7	3.4,[c] 3.7,[c] 2.7,[c] 2.7[c]	3.2[c]
	CH_2/GalNAc-H1	> 3.4	4.75,[c] 3.4,[c] 6.2,[c] 3.6[c]	4.0[c]
3	HL/CHD-H4	> 3.4	3.9, 3.6, 3.5	4.2
	HL/CHD-H3	2.4–3.0	1.9, 1.9, 1.9	2.5
	HL/CHD-H2eq	2.3–2.9	2.9, 3.3, 3.4	2.2
	HL/GalNAc-H1	> 3.4	4.7, 4.6, 3.7	4.2
	MeL/GalNAc-H1	> 3.4	3.8,[d] 3.4,[d] 3.2[d]	3.8[d]
	MeL/CHD-H2eq	3.1–3.5	5.0,[d] 5.2,[d] 5.1[d]	3.4 [d]
	MeL/CHD-H3	2.4–3.0	3.5,[d] 3.9,[d] 4.2[d]	3.9[d]
	MeL/CHD-H4	3.0–3.4	3.7,[d] 3.3,[d] 4.2,[d]	4.7[d]
4	HL/CHD-H4	2.4–3.0	3.2, 3.3	2.5,[e] 2.6,[f] 4.1[g]
	HL/CHD-H3	2.3–2.9	1.9, 1.9	2.5,[e] 2.4,[f] 2.3[g]
	HL/CHD-H2eq	2.7–3.3	3.5, 3.4	4.2,[e] 3.0,[f] 2.6[g]
	HL/GalNAc-H1	> 3.4	4.5, 3.7	2.7,[e] 2.8,[f] 4.4[g]
	MeL/GalNAc-H1	n.c.[h]	6.0,[d] 4.5[d]	4.9,[d,e] 4.5,[f] 3.8[g]
	MeL/CHD-H2eq	2.9–3.3	3.6, 3.8	3.4,[d,e] 3.6,[f] 4.0[g]
	MeL/CHD-H3	2.7–3.0	3.8, 3.9	2.7,[e] 3.1,[f] 4.4[g]
	MeL/CHD-H4	> 3.4	5.3, 5.3	4.5,[e] 4.7,[d] 5.1[g]

[a] Distances from lowest energy members of clusters in Table 3. [b] Calculated from $< r^{-6} >$ monitored during 1 ns MC/SD simulations (MDDI option of Batchmin). [c] Average over the two isochronous protons. [d] Average over the three methyl protons. [e] Simulation 1: 1 ns simulation starting from lowest Autodock score. [f] Simulation 2: 1 ns simulation starting from NMR-suggested conformer. [g] Simulation 3: as simulation 2, with lower parabolic constrain for water molecule at site 2 (see text). [h] n.c. = no connectivity observed.

site with low affinity (in the mM range),[7, 23] and the MC/EM calculations yielded many unrealistic structures. Since the NMR results clearly show that the galactose-binding site is indeed occupied by the Gal ring of **2**–**4**, MacroModel calculations (MC/EM and MC/SD) can be run by excluding this part of the molecule from the explicit Monte Carlo degrees of freedom. Such MacroModel calculations were in fact performed (see Supporting Information); however, to get a more comprehensive view of the possible binding modes, the initial docking studies of **2**–**4** were performed by using Autodock. Autodock has recently been validated for use with LT complexes by Verlinde et al.[24] who have worked out a viable protocol that is capable of predicting the correct binding mode of carbohydrate derivatives within 1 Å from experiment. Our calculations were performed by using essentially the same protocol, and retaining the two crystallographic water molecules at sites 2 and 3. Autodock results are obtained as docking solutions from multiple Monte Carlo runs. The solutions are clustered by using geometrical RMS deviation (1.5 Å), and each cluster is represented by its lowest-energy member and ranked according to the energy of the latter. Within Autodock, the energy of the complex is obtained by adding the internal steric energy of the ligand to the interaction energy that the ligand makes with the protein residues. Therefore, Autodock energies represent a score that is not directly related to a binding constant. Within 3 kcal mol^{-1}, four clusters are found for **2**, three for **3**, and only two for **4** corresponding to different poses of the ligands within the protein cleft (Table 3).

As expected on the basis of Verlinde's report,[24] Autodock performs remarkably well in the identification of the Gal-binding site, which is recognized and reproduced correctly in all low-energy clusters. In all cases, the galactose ring of **2**–**4** interacts strongly with the protein, in accordance with the NMR results, and is located in the area above the Trp-88 side chain, which is the known binding site for all the complexes formed by the two bacterial enterotoxins with Gal-containing ligands (Figure SI1–SI3 in Supporting Information). Additionally, Autodock also selects the *syn* conformer of the Gal$\beta(1\rightarrow3)$GalNAc$\beta(1\rightarrow4)$CHD pseudo-trisaccharide fragment (see Table 3). Again, this feature is amply supported by the TR-NOE observations discussed above. The clusters differ mainly by the conformation of the hydroxyacid side chain, and/or by the overall orientation of the ligand within the protein (its pose), which is most dramatically reflected in the orientation of the carboxy group. The Autodock low-energy clusters are described in detail in the Supporting Information. Interproton distances for the hydroxyacid fragment calculated from Autodock results are collected in Table 2 together with NOE values. In general, Autodock tends to support nonidealized quasieclipsed χ values (Table 3), which are reflected in unrealistically short HL/CHD-H3 distances.

A more refined model was sought by using the Autodock results as starting points for MacroModel's MC/SD calculations.[25] MC/SD mixes a molecular dynamics simulation with Monte Carlo internal coordinate movements, and thus allows

Table 3. LT complexes of **2**–**4**. Docking results (Autodock).

Ligand	No. of clusters[a]	Rank of clusters[b]	Members in cluster	Lowest energy in cluster [kcal mol^{-1}][c]	Ligand conformation A[d]	B[e]	C[f]
2	24	1	38	– 61.18	38, – 36	26,– 8	– 108, – 6 (– 97)
		2	24	– 59.57	24,5	25,36	– 118, – 19 (– 119)
		3	7	– 58.44	32, – 1	– 20, – 44	– 160,34 (– 116)
		4	17	– 58.16	19, – 36	24,– 14	– 158,34 (– 113)
3	30	1	6	– 65.55	47, – 28	44,4	137,11 (131)
		2	28	– 64.69	30, – 37	27,– 2	139, – 5 (117)
		3	19	– 64.32	57, – 19	33,37	102,8 (95)
4	24	1	25	– 67.61	45, – 38	33,– 13	– 124, – 5 (– 112)
		2	48	– 66.62	51, – 17	43,26	– 115, – 7 (– 105)

[a] Clustering of a total of 128 runs. [b] Clusters within 3 kcal mol^{-1} of lowest Autodock score. [c] Autodock scores. [d] Gal-GalNAc ϕ,ψ. [e] GalNAc-CHD ϕ,ψ. [f] Hydroxyacid-CHD ϕ,ψ (χ).

© 2002 WILEY-VCH Verlag GmbH & Co. KGaA, Weinheim
0947-6539/02/0820-4606 $ 20.00+.50/0 *Chem. Eur. J.* **2002**, *8*, No. 20

one to explore conformational space more effectively than by using dynamics alone. For the study of the LT:ligand complexes, the protocol discussed at the beginning of this section was used, that is, the hydroxyacid side chain bonds were used as Monte Carlo variables, while the pseudo-trisaccharide fragment was not explicitly varied in the Monte Carlo steps. Furthermore, the ligand was allowed to rotate and translate in the protein binding site, so as to optimize its pose.

A 1 ns MC/SD simulation of the LT:**2** complex (glycolic acid derivative) was run starting from the lowest score Autodock pose, which features a $\phi,\psi = -108°, -6°$ ($\chi = -97°$) hydroxyacid–CHD junction (see Table 3). The closest MMOD minimum is located at $\phi,\psi = -160°, -30°$ ($\chi = -178°$), and this conformation is maintained for the first 30 ps of the simulation (Figure 7). After this time, a transition

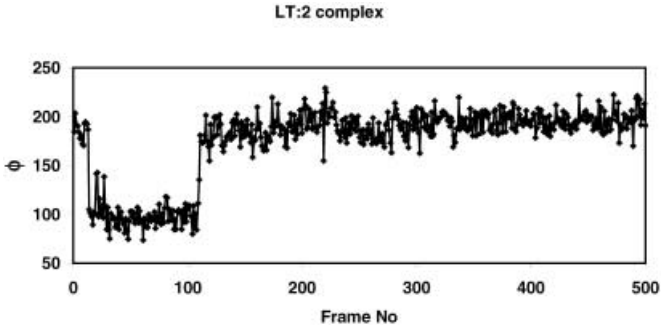

Figure 7. MC/SD simulation (1 ns) of the LT:**2** complex. The glycolic acid side chain ϕ torsion is plotted against the number of the saved frame. Frames were saved every 2 ps during the simulation.

occurs to a $\phi,\psi = 90°,50°$ ($\chi = 154°$) conformer of the glycolic acid side chain in which the carboxy group hydrogen bonds to the backbone NH of Arg-13. This is the same orientation reached in the Autodock clusters 3 and 4, although the ligand conformation is different (see Table 3). After approximately 120 ps, a new transition occurs back to the starting conformer, which is conserved for the rest of the simulation. This behavior qualitatively agrees with the available NMR observations, which are consistent with the prevalence of the $\chi = 180°$ conformer. The calculated interproton distances (Table 2, MMOD column) are improved relative to the Autodock results, but HL/CHD-H2eq is still too long.

When the same simulation was run for the LT:**3** complex ((*R*)-lactic derivative, Figure 8), no stable transitions were observed in the side chain ϕ value, but frequent fluctuations occurred between two conformations at $\phi = 70°$ and $\phi = 115° \pm 8°$, with occasional spikes at $\phi = 170°$. Somewhat larger variations are observed for the ψ torsion (Figure 8b). However, $\chi = 150° \pm 20°$ for more than 95% of the saved frames, and the carboxy group remains firmly oriented towards the Arg-13 backbone NH to which it is hydrogen bonded for the whole simulation. The model emerging from the MC/SD simulation (see Figure 10) is in agreement with the TR-NOE results that exhibit a strong interaction between the lactic acid side chain proton HL and CHD-H2eq (Table 2). Thus, two low-energy conformations of the (*R*)-lactic derivative **3** ($\phi,\psi = 90°,80°$ and $120°,10°$) that both feature a distorted χ *anti*-type conformation (Table 4) appear to be selected from

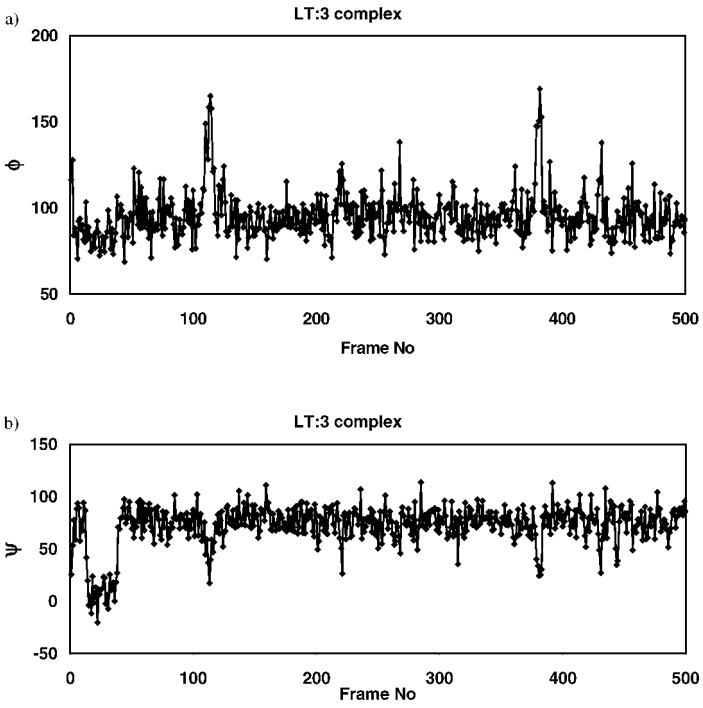

Figure 8. MC/SD simulation (1 ns) of the LT:**3** complex. a) The (*R*)-lactic acid side chain ϕ torsion is plotted against the number of the saved frame. b) The (*R*)-lactic acid side chain ψ torsion is plotted against the number of the saved frame. Frames were saved every 2 ps during the simulation.

the available free state pool. Compared to the free state calculations that yielded a 90:10 $\chi = +40°/\chi = +150°$ ratio, MMOD appears to reproduce the conformational selection that occurs during the binding event (Table 4). The $\chi = -60°$ conformation is never attained during the simulation; the HL/CHD-H2eq distance is in fact slightly too short and the Me/CHD-H2eq distance is too long relative to experimentally measured values.

According to the NMR studies, the $\chi = -60°$ conformation should be more represented in the LT:**4** complex, and thus it should be more easily found by the calculations. However, Autodock calculations do not find the $\chi = -60°$ conformer as a low-score conformer. Macromodel's MC/SD simulation starting from the lowest Autodock score pose ($\phi,\psi = -124°, -5°$; $\chi = -112°$, see Table 3) reaches the $\chi = 180°$ conformation ($\phi = 180°$; $\chi = 180°$) upon MMOD minimization and stays there (Figure 9a, Table 2 simulation 1) for the duration of the simulation (1 ns). If the starting conformation is switched to the $\chi = -60°$ conformer (Me antiperiplanar to CHD-C3, $\phi = -60°$, Figure 9b and simulation 2 in Table 2), a transition to the $\phi = 180°$ conformer is observed after around 360 ps. This is in striking contrast with the Macromodel results for the free state that yielded only one low-energy conformer at $\chi = -60°$. However, the side chain flexibility of the computational model for the bound state appears to be critically dependent on the computational treatment of the crystallographic water molecule at site 2. Hydrogen bonding interaction between this water molecule and the ligand carboxylate group stabilizes the $\chi = -60°$ conformation of **4** in the calculations of the bound state. If this water molecule is left more free to adjust its position during the simulation by

Table 4. Favored idealized conformations of hydroxyacid side chain in **2**–**4** based on NMR data.

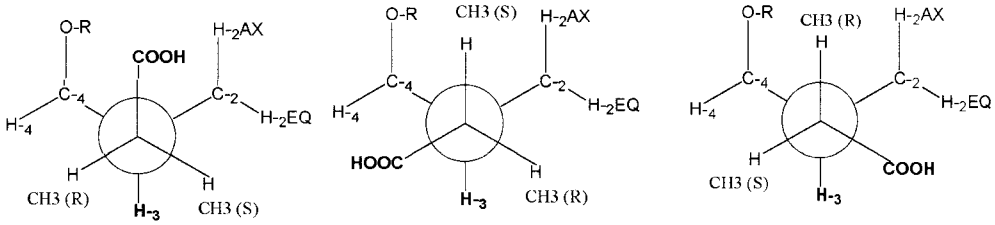

	χ 180°		- 60°		+ 60°	
Compound	Free state χ [°]		Bound state χ [°]			K_D[a]
	NMR	MMOD (Kolb, MC/EM)[b]	NMR	Autodock (MC/SD)	MMOD	[μM]
2	180 (major) +60 (minor)	−50 (ca. 90%) +40 (ca. 10%)	180 (major) −60 (minor)	−97, −119, −116, −113	180 ± 40	700
3	+60 (major) 180 (minor)	+40 (ca. 90%) +150 (ca. 10%)	180 (major) −60 (minor)	131, 117, 95	150 ± 20	190
4	180 (major) −60 (minor)	−50	180 (major) −60 (minor)	−112, −105	180 ± 30 (70%)[c] −60 ± 30 (30%)[c]	1000

[a] From ref. [4]. [b] Boltzmann distribution within 3 kcal mol^{-1} from global minimum. [c] Best agreement with experiment.

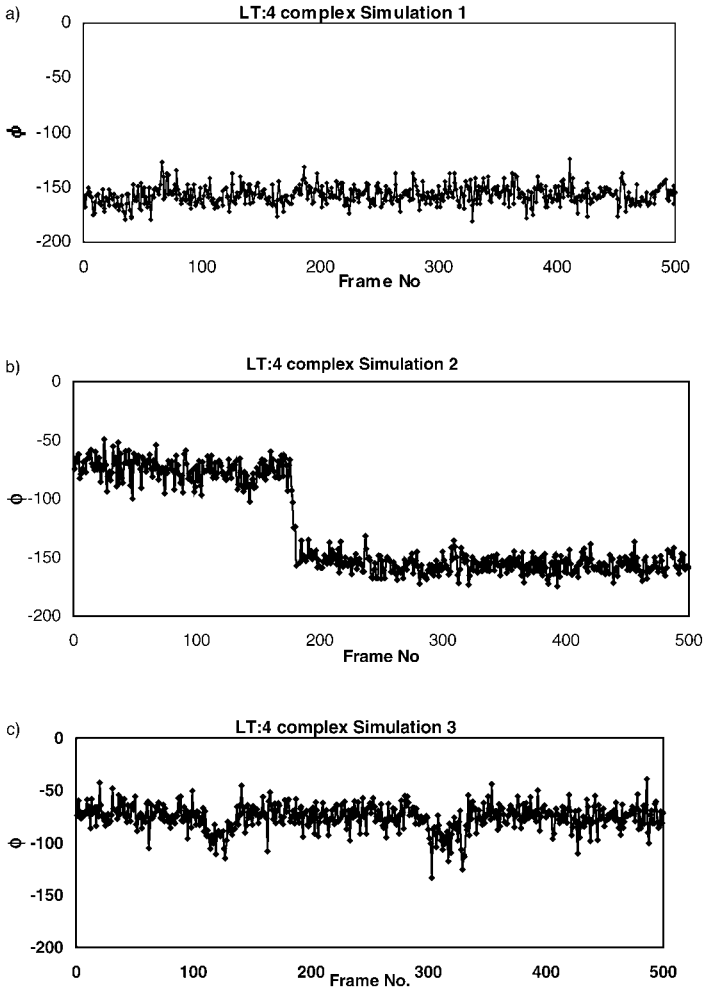

Figure 9. MC/SD simulations (1 ns) of the LT:**4** complex. The (*S*)-lactic acid side chain ϕ torsion is plotted against the number of the saved frame. Frames were saved every 2 ps during the simulation. a) Simulation 1 was run starting from the lowest score Autodock pose ($\chi = 180$). b) Simulation 2 was run starting from the $\chi = -60$ conformation. c) Simulation 3 as simulation 2, lowering the parabolic restraint on crystallographic water at site two.

lowering the parabolic restraint on its oxygen atom (i.e., moving it from shell 2 to shell 1 in the MacroModel substructure calculation), the $\chi = -60^\circ$ conformation appears to be stable for the entire simulation time (Figure 9c and simulation 3 in Table 2). The best agreement with the NOE data is obtained in simulation 2, which consists of around 30% of the $\chi = -60^\circ$ conformation together with 70% of the $\chi = 180^\circ$ conformation. Once more this warns against interpretation of NOE results in carbohydrate and glycomimetic complexes based on a single conformation, and demonstrates that with these flexible molecules reproduction of dynamic data can actually be rather tricky.

In conclusion, the computations clearly agreed with the experimental observation that a common $\chi = 180^\circ$ conformation is adopted by all three mimics in the bound state. Some residual conformational freedom of the hydroxyacid side chain seems to be supported by the NMR results, and the calculations suggest that it may be correlated to critical interactions between the carboxylate group and the water molecule at crystallographic site 2. The common ligand pose in the toxin binding site, very similar to the orientation of the natural ligand o-GM1, is represented for the LT:**3** complex in Figure 10.

Discussion and Conclusion

The structure of the CT:o-GM1 complex was established by X-ray crystallography.[5] The data show that the terminal Gal moiety of GM1 inserts rather deeply into CT binding cleft and makes hydrophobic contacts to the Trp-88 side chain, while establishing a tight hydrogen bonding network around its β-face. The other important contact between toxin and substrate is made by the NeuAc carboxy group, which hydrogen bonds to Trp-88 through a highly conserved crystallographic water molecule (W3, at site 3). A second X-ray water molecule (W2, at site 2) is found near the sialic acid side chain, and mediates

© 2002 WILEY-VCH Verlag GmbH & Co. KGaA, Weinheim
0947-6539/02/0820-4608 $ 20.00+.50/0 *Chem. Eur. J.* **2002**, *8*, No. 20

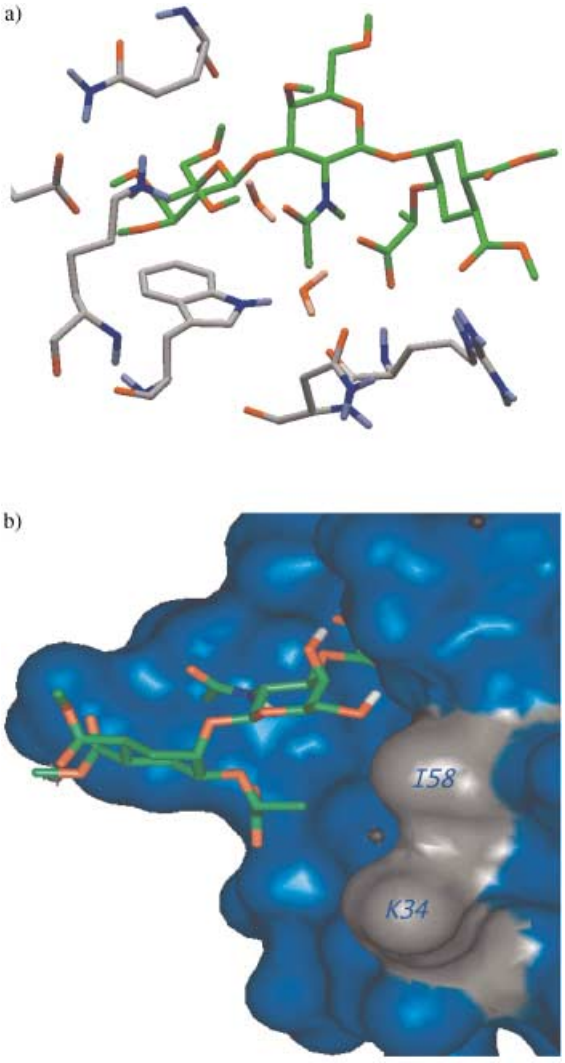

Figure 10. LT:**3** complex as calculated by MacroModel. a) Detailed view of the binding site. The ligand **3** is in green, the protein residues involved in the interaction are in grey. b) The ligand **3** is in green, and the protein surface is blue. The hydrophobic patch identified by the DRY probe of GRID near 158 and K34 is in gray.

hydrogen bonding from Gal-OH6 and NeuAc-OH7 to Gly-33. We previously demonstrated that conserving this water molecule is essential to computationally reproduce the experimental CT:o-GM1 structure.[22] W2 is also highly conserved in the X-ray structure of CT, LT, and many of their sugar complexes. However, Verlinde and co-workers have shown that this molecule can be displaced by some Gal-based LT-binders.[23] GRID calculations, also reported by Verlinde[24] and confirmed by us (see Experimental section), indicate that W2 sits near a relatively high-energy minimum for the water probe. In the CT:o-GM1 X-ray structure, the conformation of the bound ligand is the same in all five independent CT sites: the Gal$\beta(1\rightarrow3)$GalNAc$\beta(1\rightarrow4)$Gal fragment is in the *syn,syn* conformation. The sialic acid has a $\phi,\psi=-169^\circ,-31^\circ$ conformation, which corresponds to $\chi=166^\circ$. This conformation is the same as that determined by NMR studies of GM1[26] and psGM1 **1**,[3] and reproduced by the MacroModel calculations.[3, 19] Indeed, the conformational stability of the Gal$\beta(1\rightarrow3)$GalNAc$\beta(1\rightarrow4)$Gal trisaccharide and its GalNAc$\beta(1\rightarrow4)$Gal fragment appears to be conserved in all known ganglioside structures (GM1, GM2, asialoGM1).[19] In contrast, the sialic acid in the NeuAc$\alpha(2\rightarrow3)$Gal fragment can assume two orientations at $\chi=-60^\circ$ or $\chi=180^\circ$. The two conformations are almost equally represented if the Gal-O4 is not substituted (as in GM4[19, 27] and GM3,[19, 28] or in sialyl Lewis-X[29]); however, the $\chi=180^\circ$ conformation is stabilized in the Gal-O4-branched gangliosides GM1, GM2, and psGM1 **1**.[3, 19, 26, 30]

The CT galactose-binding site is probably exploited by **2**–**4**, as suggested by both the large decrease in Trp-88 fluorescence emission observed upon binding to CT,[4] and by the STD experiments described above, which implicate a close proximity between CT and the Gal fragment of the ligands. It is evident from the analysis of the CT:o-GM1 X-ray structure that optimal toxin binding can be achieved if the proper relative orientation of the terminal Gal and the ligand carboxy group is attained. Previous work on psGM1 **1**[3] has revealed that the Gal$\beta(1\rightarrow3)$GalNAc$\beta(1\rightarrow4)$CHD fragment shares the same conformation and conformational stability of the parent Gal trisaccharide; thus, in the derived mimics the conformation of the carboxylate-bearing chain should define the toxin affinity. Indeed, the NMR work presented here clearly shows that similar (*syn*) conformations around the Gal and GalNAc glycosidic bonds of mimetics **2**–**4** are present in the free state and are recognized by cholera toxin. The analysis of the hydroxyacid side chain emerging from the NMR data can be summarized on the basis of the idealized improper dihedral angle χ (Figure 3) as shown in Table 4.

Based on the above models and on the NMR data, the different affinity of the three ligands cannot be interpreted in a straightforward manner. However, it is very intriguing to compare their behavior with that of ganglioside GM1, which was used for the initial design of these molecules. Based on the structure of the CT:o-GM1 complex, our expectation was that complex formation would occur by using the $\chi=180^\circ$ conformation of the hydroxyacid chain. Indeed, the computational models and the TR-NOE data of the bound state are consistent with nonidealized $\chi=180^\circ$ conformations for all three compounds (**2**: $\chi=180^\circ\pm40^\circ$; **3**: $\chi=150^\circ\pm20^\circ$; **4**: $\chi=180^\circ\pm40^\circ$). The presence of minor $\chi=-60^\circ$ conformers is also suggested by NMR analysis. MC/SD calculations of the (*S*)-lactic acid derivative **4** strongly suggest that this conformation may involve interaction of the side chain carboxy group with crystallographic water W2, and may be simulated by MacroModel, depending on the computational treatment of crystallographic water molecules.

Thus, the NMR study reveals that the strongest binder of the series, the (*R*)-lactic derivative **3**, binds mostly in its minor free state conformation ($\chi=180^\circ$), whereas the (*S*)-lactic derivative **4** (which is approximately fivefold less potent than **3**) and the glyco derivative **2** (which is around threefold less potent) both use their free state global minimum. Hence, the observed differences in binding affinity cannot be attributed to preorganization, which should favor **2** and **4** over **3**, but must originate from some other factor(s). Given the similar conformation adopted by natural and unnatural ligands, and considering the C-2 configuration of NeuAc, comparison with GM1 also indicates that the side chain methyl group of **4**

 © 2002 WILEY-VCH Verlag GmbH & Co. KGaA, Weinheim 0947-6539/02/0820-4609 $ 20.00+.50/0

points in the same direction as the sialic acid C-3 (CH_2); thus, its lower affinity should not arise from steric hindrance or bad contacts with the protein. Although merely speculative, the higher affinity of the *R* derivative **3** could be attributed to the establishment of lipophilic interactions between the toxin cleft and the methyl group of **3**, which points in the direction occupied by the NeuAc side chain in the CT:o-GM1 structure (Figure 10b). Indeed, from the GRID analysis of the CT:o-GM1 complex described in the Experimental section, a deep minimum for the DRY probe was found near the tail of the sialic acid glycerol fragment, which is close to I58 and K34 (Figure 10b). These two residues appear to form a lipophilic patch in the toxin, which has also been exploited for the design of artificial ligands.[31] This information strongly suggests that the affinity of the pseudo-GM1-based binders may be improved by filling this cavity with appropriate hydrophobic fragments linked to the (*R*)-lactic acid o-GM1-mimic. Work is in progress toward this end in our laboratories.

Similar (*syn*) conformations of the glycosidic bonds in the Gal$\beta(1\rightarrow3)$GalNAc$\beta(1\rightarrow4)$CHD pseudo-trisaccharide of o-GM1 mimics **2**–**4** are recognized by cholera toxin. Moreover, the protein selects one or two side chain conformations for the hydroxyacids (lactic, glycolic) used as NeuAc analogues; the preferred conformation is that in which the COOH group is *anti* to the C3 of the CHD moiety ($\chi = 180^\circ$). Since these chains present several low-energy conformations in water solution, the reported observations represent an instructive case of conformer selection by a lectin binding site. For cholera toxin, the binding site architecture allows the global energy minima around the glycosidic linkages of mimetics **2**–**4** to be accommodated with minor variations of the torsion angles. From a general point of view, and in relation to other results for different protein-bound oligosaccharides, it becomes clear that the selection of a conformer from an equilibrium mixture appears to prevail relative to distorting angles of free solution conformers. This conclusion is not trivial and is underscored by noting that for carbohydrates it is not infrequent that even minor conformers are able to function as ligands. As an example, the *anti-*ψ and *anti-*ϕ (*gauche*–*gauche*) conformations of *C*-lactose are selected by ricin-B[32] and *E. coli* β-galactosidase,[33] respectively. When two conformations are possible in the central *syn* valley, they can be differentially selected with obvious implications for design of target-selective drugs. It is notable that even in these cases with no or only minor differences in energetic content, the documented NMR-based approach is valuable to define the topology of the bound ligand and to underscore entropic factors reducing affinity.

Experimental Section

Ligands: The synthesis of compounds **2**–**4** has been reported in a previous communication;[4] their characterization is reported in the Supporting Information of this paper.

NMR experiments: NMR spectra were recorded at 25–30 °C in D_2O, on Varian Unity 500 MHz and Bruker AVANCE 500 MHz spectrometers. For the experiments with the free ligands, the corresponding compound (2–5 mg) was dissolved in D_2O, and the solution was degassed by flushing with argon. COSY, TOCSY (80 ms, mixing time), and ge-HSQC experiments were performed by using standard sequences at temperatures between 298 and 310 K. For selective one-dimensional NOESY, the double pulse field gradient echo sequence proposed by Shaka[34] was used with mixing times of 200, 400, and 600 ms. Two-dimensional T-ROESY experiments[35] were also performed with mixing times of 300 and 500 ms. The strength of the 180 pulses during the spin lock period was attenuated four times with respect to that of the 90 hard pulses (between 7.2 and 7.5 μs). To deduce the interproton distances, relaxation matrix calculations were performed by using software written in-house, which is available upon request from the authors.[36]

For the bound ligands, STD[37] and TR-NOE experiments[38] were performed. The cholera toxin CTB pentamer was purchased from List Biological Laboratories Inc. The commercial sample was ultrafiltered and subjected to two cycles of freeze-drying with D_2O to remove traces of H_2O before transferring it in solution to the NMR tube to give a final concentration of approximately 0.1–0.2 mM. TR-NOESY experiments were performed with mixing times of 100, 200, and 300 ms, for molar ratios between 15:1 and 50:1 of glycoside/lectin. Selective one-dimensional TR-NOESY experiments were also performed by using the same double pulse field gradient echo with mixing times of 300 ms. No purging spin lock period was employed to remove the background protein signals. First, in all cases, line broadening of the sugar protons was monitored after the addition of the ligand. STD experiments were carried out by using the method proposed by Meyer[20] and Peters.[21] No saturation of the residual HDO signal was employed and, again, no spin lock pulse was employed to remove the background protein signals. In our hands, the use of a spin lock period induced artifacts in the difference spectrum.

The theoretical analysis of the TR-NOEs of the sugar protons was performed according to the protocol employed by London, using a relaxation matrix with exchange as described.[39] Different exchange-rate constants (k), defined as $pf \times k = K_{-1}$ (in which pf is the fraction of the free ligand), and leakage relaxation times were employed to obtain the optimal match between experimental and theoretical results of the intraresidue H-1/H-3 and H-1/H-5 cross peaks of the Gal and GalNAc moieties for the given protein/ligand ratio. Normalized intensity values were used since they allow correction for spin-relaxation effects. The overall correlation time τ_c for the free state was always set to 0.15 ns, and the τ_c for the bound state was estimated as 15 ns according to the molecular weight (M_r) of the lectin ($\tau_c = 10^{-12} M_r$). To fit the experimental TR-NOE intensities, exchange-rate constants between 100 and 1000 s^{-1}, and external relaxation times ρ^* for the bound state of 0.5, 1, and 2 s were tested. Optimal agreement was achieved when using $k = 150\ s^{-1}$ and $\rho^* = 1$ s. Only the protons of the ligand were included in the calculations, due to the lack of precision in unambiguously detecting the position of the protein protons.

T-ROESY experiments were also carried out to exclude spin-diffusion effects.[40, 41] A continuous wave spin lock pulse was used during the 250 ms mixing time. Key NOEs were proven to be direct cross peaks, since they had different signs relative to diagonal peaks. In some cases, they allowed the detection of intra-Gal and intra-GalNAc H1/H4 and H1/H6 cross peaks resulting from spin diffusion.

Computational methods. Conformational search and dynamics of isolated 2–4: The calculations were performed by using the MacroModel/Batchmin[42] package (version 5.5) and the AMBER* force field. Kolb's parameters were used for the hydroxyacid moiety.[18] Bulk water solvation was simulated by using MacroModel's generalized Born GB/SA continuum solvent model.[43] This model treats the solvent as an analytical continuum starting near the van der Waals surface of the solute, and uses a dielectric constant of 78 for the bulk water and 1 for the molecule.

The conformational searches were carried out by using 20000 steps of the usage-directed MC/EM procedure following previously established protocols.[22, 19] Extended nonbonded cut-off distances (a van der Waals cut-off of 8.0 Å and an electrostatic cut-off of 20.0 Å) were used. The interatomic distances reported in Table 1 are $\langle r^{-6} \rangle^{-1/6}$, in which $\langle r^{-6} \rangle$ is the Boltzmann average of the r_i^{-6} of the individual conformations within 3 kcal mol^{-1} of the global minimum.

For the MC/SD[25] dynamic simulations, van der Waals and electrostatic cut-offs of 25 Å, together with a hydrogen bond cut-off of 15 Å were used. This extension of the standard MacroModel/Batchmin values (8, 20, and 4 Å, respectively) slowed the calculation down, but allowed for a smoother convergence, avoiding the strong increments of the energy that can arise

 © 2002 WILEY-VCH Verlag GmbH & Co. KGaA, Weinheim 0947-6539/02/0820-4610 $ 20.00+.50/0 *Chem. Eur. J.* **2002**, *8*, No. 20

from significant conformational changes. The dynamic simulations were run by using the AMBER* all-atom force field. The same degrees of freedom of the MC/EM searches were used in the MC/SD runs. All simulations were performed at 300 K, with a dynamic time-step of 1.5 fs and a bath constant τ of 0.2 ps. Typically, two runs of 3 ns each were performed, starting from two conformations of the substrates, selected from the MC/EM outputs, which differed at the hydroxyacid linkage. The Monte Carlo acceptance ratio was about 4%; each accepted MC step was followed by an SD step. Structures were sampled every 6 ps and saved for later evaluation. Convergence was checked by monitoring both energetic and geometrical parameters. In general, when the simulations were stopped, the interproton distances and the conformer populations determined by each run differed by no more than 0.1 Å and 5–6%, respectively. The interatomic distances reported in Table 1 were evaluated from $< r^{-6} >$ monitored during the simulation (option MDDI of Batchmin).

Conformational search (MC/EM) of the LT:3 complex: The conformational searches were carried out by using the usage-directed MC/EM procedure, with slight variations of the protocol used in the study of the LT:psGM1 complex.[3] In brief, the starting structure was obtained by graphical modification of the LT:**1** complex, followed by substructure energy minimization. Five explicit torsional variables were included: the C5–C6 bonds of Gal and GalNAc, and the three bonds of the hydroxyacid moiety. Explicit MC variable did not include the Gal–GalNAc and Gal–DCCHD anomeric linkages. Due to the relatively low binding constant, the ligand tends to wander out of the toxin site when these variables are included.[22] However, the ligand was allowed to rotate (max. 180°) and translate (max. 1 Å) within the binding site (MOLS command of Batchmin); 11000 MC/EM steps were performed. Bulk water solvation was simulated by using the GB/SA model. Five crystallographic water molecules were retained, as previously described.[3, 22] All calculations were carried out on a B_2 (B + B(+1)) dimer. Only the ligand and a shell of residues surrounding the binding site of LT were subjected to energy minimization. All the residues within 5 Å of the sugars were included in the shell. The ligand and all polar binding site hydroxy and amino hydrogens were unconstrained during energy minimization. All other atoms that belonged to the substructure being minimized were constrained to their crystallographic coordinates by parabolic restraining potentials that increased with the distance from the sugar substrate. The following force constants were used: 100 kJ Å^{-2} for the atoms within 0–3 Å of any atom of the ligand; 200 kJ Å^{-2} for the atoms within 3–4 Å; 400 kJ Å^{-2} for the atoms within 4–5 Å. The periphery of the restrained structure was checked with the EdgeD command of MacroModel, and isolated atoms were included to avoid incomplete functional groups. All other atoms were ignored. The results are described in the Supporting Information.

MC/SD dynamics of the LT:ligand complexes: The simulations were carried out by using the same substructure and explicit MC variables described above, and starting from the lowest energy conformation from the MC/EM search (for the (*R*)-lactic derivative **3**) or from the lowest score Autodock pose. Extended nonbonded cut-offs were employed (van der-Waals and electrostatic 25 Å, hydrogen bond 15 Å). The simulations were performed for 1 ns, at 300, with a dynamic time-step of 1.5 fs and a bath constant τ of 0.2 ps. The Monte Carlo acceptance ratio was about 36%; each accepted MC step was followed by a SD step. Structures were sampled every 2 ps and saved for later evaluation. The interatomic distances reported in the Table 2 were evaluated from $< r^{-6} >$ monitored during the simulation (option MDDI of Batchmin).

Docking studies. Protein subset construction: The crystal complex of CT-B_5 pentamer bound to o-GM1 (2chb.pdb)[5] and *E. coli* LT with lactose (1ltt.)[44] were superimposed by using their C_α atoms within InsightII.[45] 1ltt protein residues and the crystal water molecules lying within 15 Å from each atom of GM1 (2chb) were collected to generate the o-GM1:LT complex. Polar hydrogens of the protein residues were added with the *polH* routine (AUTODOCK 2.43[46]) and their orientation was optimized within Macromodel 5.0[42] by energy minimization (AMBER force field) followed by 1000 steps of Monte Carlo/energy minimization using BatchMin. While charges fitted to the electrostatic potentials were generated for the ligands (MNDO hamiltonian, ESP keyword, MOPAC6), those of the protein residues were assigned with *q.kollua* routine provided with AUTODOCK 2.43.

Docking studies: Docking studies of **2**–**4** within the protein subset were performed with AUTODOCK 2.43.[46] Crystal water molecules 2 and 3 were retained as they appear to be conserved throughout the whole set of crystal complexes available for these proteins. Affinity grid files were generated using a grid $22.5 \times 22.5 \times 22.5$ Å^3 wide for (*R*)-lactic acid and $21 \times 21.5 \times 15.5$ for glycolic and (*S*)-lactic derivatives at 0.375 Å resolution. Twenty torsions were allowed to vary during the simulation using the Gal residue as the root fragment. The parameters for AUTODOCK Monte Carlo/simulated annealing protocol were the same for all docking simulations. The maximum number of allowed runs (128) was set. Each run consisted of 110 cycles of simulated annealing steps during which the temperature was gently relaxed from 310 K in the first cycle using a temperature reduction factor of 0.95 cycle^{-1}. The maximum number of accepted and rejected trials per cycle was set to 30000. Then, the 128 solutions obtained were clustered according to RMS deviations lower than 1.5 Å. Each cluster was ranked by the lowest energy representative of each cluster, which was selected as representative of the cluster.

GRID analysis: The GRID[47] (version 17) program was used to characterize the protein active site properties. This investigation allowed us to spot the most favorable regions for hydrophilic/hydrophobic interactions that can be exploited in the design of novel GM1-receptor mimics. OH2 (water), OH (phenol OH), O1 (alkyl hydroxyl oxygen), COO− (carboxylic acid), C3 (methyl), and (DRY) hydrophobic probes were placed at the nodes of a grid $69 \times 91 \times 85$ Å^3 wide (0.5 Å spacing) laid over the binding site of lactose/GM1 binding site (533715 points). Both the crystal water molecules and the ligand were removed. Minima were found by application of MINIM program followed by annealing with FILMAP routine. Grid maps were visualized within InsightII-(Accelrys). Deep minima for the OH2 probe were found in close proximity to the crystal water sites 1, 3, and 5 as well as to the hydroxyl groups of the Gal fragment. A minimum was also found near water site 2 at a higher energy level. While minima of O1 map are close to the conserved crystal water sites as well as to the hydroxyl groups of the sugars, those of COO− probe lie in the vicinity of the carboxyl group of GM1 sialic acid. While a wide hydrophobic region was spotted with C3 probe near Gal and crystal water molecules, DRY minima are located essentially where the Gal sits, which confirms that the sugar ring makes hydrophobic interactions with the indole of the W88 residue. In addition, a deep minimum was found near the tail of the sialic acid glycerol fragment, which is close to I58 and K34.

Acknowledgements

Financial support from DGICYT (BQU2000–1501-C01), CILEA (Centro di Modellistica Computazionale), MURST (COFIN2000 prot. MM03155477), CNR, the exchange program between Spain and Italy (Acciones Integradas-Azioni Integrate) and the COST D-13 program are gratefully acknowledged. A.G.H. thanks Gobierno Vasco for a fellowship.

[1] P. Sears, C. H. Wong, *Angew. Chem.* **1999**, *111*, 2446–2471; *Angew. Chem. Int. Ed.* **1999**, *38*, 2300–2324, and references therein.
[2] A. Bernardi, G. Boschin, A. Checchia, M. Lattanzio, L. Manzoni, D. Potenza, C. Scolastico, *Eur. J. Org. Chem.* **1999**, *6*, 1311–1317.
[3] A. Bernardi, P. Brocca, A. Checchia, S. Sonnino, F. Zuccotto, *J. Am. Chem. Soc.* **1999**, *121*, 2032–2036.
[4] A. Bernardi, L. Carrettoni, A. Grosso Ciponte, D. Monti, S. Sonnino, *Bioorg. Med. Chem. Lett.* **2000**, *10*, 2197–2200.
[5] E. A. Merritt, S. Sarfaty, F. van den Akker, C. L'Hoir, J. A. Martial, W. G. J Hol, *Protein Sci.* **1994**, *3*, 166–175.
[6] C.-L. Schengrund, N. J. Ringler, *J. Biol. Chem.* **1989**, *264*, 13233–13237.
[7] J. A. Mertz, J. A. McCann, W. D. Picking, *Biochem. Biophys. Res. Comm.* **1996**, *226*, 140–144.
[8] A. A. Bothner-By, R. Gassend, *Ann. N. Y. Acad. Sci*. **1973**, *222*, 668–676.
[9] P. L. Jackson, H. N. Moseley, N. R. Krishna, *J. Magn. Res. B* **1995**, *107*, 289–292.
[10] V. L. Bevilacqua, D. S.Thomson, J. H. Prestegard, *Biochemistry* **1990**, *29*, 5529–37; V. L. Bevilacqua, Y. Kim, J. H. Prestegard, *Biochemistry* **1992**, *31*, 9339–9349.
[11] A. Poveda, J. Jimenez-Barbero, *Chem. Soc. Rev.* **1998**, *27*, 133–143.

 © 2002 WILEY-VCH Verlag GmbH & Co. KGaA, Weinheim 0947-6539/02/0820-4611 $ 20.00+.50/0

[12] J. Jiménez-Barbero, J. L. Asensio, F. J. Cañada, A. Poveda, *Curr. Opin. Struct. Biol.* **1999**, *9*, 549 – 555.
[13] D. Neuhaus, M. P. Williamson, *The NOE Effect in Structural and Conformational Analysis*, VCH, New York, **1989**.
[14] J. Dabrowski, T. Kozár, H. Grosskurth, N. E. Nifant′ev, *J. Am. Chem. Soc.* **1995**, *117*, 5534 – 5539.
[15] J. L. Asensio, J. Jimenez-Barbero, *Biopolymers* **1995**, *35*, 55 – 73.
[16] A. D. French, J. W. Brady, *Computer Modelling of Carbohydrate Molecules*, American Chemical Society Symposium Series, **1990**.
[17] K. Bock, J. Duus, *J. Carbohydr. Chem.* **1994**, *13*, 513 – 543.
[18] H. C. Kolb, B. Ernst, *Chem. Eur. J.* **1997**, *3*, 1571 – 1578.
[19] P. Brocca, A. Bernardi, L. Raimondi, S. Sonnino, *Glycoconj. J.* **2000**, *17*, 283 – 299.
[20] J. Klein, R. Meinecke, M. Meyer, B. Meyer, *J. Am. Chem. Soc.* **1999**, *121*, 5336 – 5337.
[21] M. Vogtherr, T. Peters, *J. Am. Chem. Soc.* **2000**, *122*, 6093 – 6099.
[22] A. Bernardi, L. Raimondi, F. Zuccotto, *J. Med. Chem.* **1997**, *40*, 1855 – 1862.
[23] W. E. Minke, C. Roach, W. G. J. Hol, C. L. M. J. Verlinde, *Biochemistry* **1999**, *38*, 5684 – 5692.
[24] W. E. Minke, D. J. Diller, G. G. J. Hol, C. L. M. J. Verlinde, *J. Med. Chem.* **1999**, *42*, 1778 – 1788.
[25] F. Guarnieri, W. C. Still, *J. Comput. Chem.* **1994**, *15*, 1302 – 1310.
[26] D. Acquotti, L. Poppe, J. Dabrowski, C. W. von der Lieth, S. Sonnino, G. Tettamanti, *J. Am. Chem. Soc.* **1990**, *112*, 7772 – 7778; P. Brocca, P. Berthault, S. Sonnino, *Biophys. J.* **1998**, *74*, 309 – 318.
[27] L. Poppe, J. Dabrowski, C. W. von der Lieth, M. Numata, T. Ogawa, *Eur. J. Biochem.* **1989**, *180*, 337 – 342; J. Schulte, J. Lauterwein, U. Höweler, *Magn. Reson. Chem.* **2000**, *38*, 751 – 756.
[28] H.-C. Siebert, G. Reuter, R. Schauer, C. W. von der Lieth, J. Dabrowski, *Biochemistry* **1992**, *31*, 6962 – 6971.
[29] R. Harris, G. R. Kiddle, R. A. Field, M. J. Milton, B. Ernst, J. L. Magnani, S. W. Homans, *J. Am. Chem. Soc.* **1999**, *121*, 2546 – 2551 and references therein.
[30] S. Sabesan, K. Block, R. U. Lemieux, *Can. J. Chem.* **1984**, *62*, 1034 – 1045; Y.-T. Li, S.-C. Li, A. Hasegawa, H. Ishida, M. Kiso, A. Bernardi, P. Brocca, L. Raimondi, S. Sonnino, *J. Biol. Chem.* **1999**, *274*, 10014 – 10018.
[31] W. E. Minke, F. Hong, C. L. M. J. Verlinde, W. G. J. Hol, E. Fan, *J. Biol. Chem.* **1999**, *274*, 33469 – 33473.
[32] J. F. Espinosa, J. L. Asensio, J. Cañada, H. Dietrich, M. Martin-Lomas, R. R. Schmidt, J. Jimenez-Barbero, *Angew. Chem.* **1996**, *108*, 323 – 326; *Angew. Chem. Int. Ed. Engl.* **1996**, *35*, 303 – 306.
[33] J. F. Espinosa, E. Montero, J. L. Garcia, H. Dietrich, R. R. Schmidt, M. Martin-Lomas, A. Imberty, J. Cañada, J. Jimenez-Barbero, *J. Am. Chem. Soc.* **1998**, *120*, 1309 – 1316.
[34] K. Stott, J. Stonehouse, J. Keeler, T. L. Hwang, A. J. Shaka, *J. Am. Chem. Soc.* **1995**, *117*, 4199 – 4200.
[35] T. L. Hwang, A. J. Shaka, *J. Am. Chem. Soc.* **1992**, *114*, 3157 – 3159.
[36] A. Poveda, J. L. Asensio, M. Martín-Pastor, J. Jimenez-Barbero, *J. Biomol. NMR* **1997**, *10*, 29 – 43.
[37] M. Meyer, B. Meyer, *Angew. Chem.* **1999**, *111*, 1900 – 1904; *Angew. Chem. Int. Ed.* **1999**, *38*, 1784 – 1788.
[38] J. L. Asensio, J. F. Espinosa, H. Dietrich, J. Cañada, R. R. Schmidt, M. Martín-Lomas, S. André, H. Gabius, J. Jiménez-Barbero, *J. Am. Chem. Soc.* **1999**, *121*, 8995 – 9000; T. Haselhorst, J. F. Espinosa, J. Jiménez-Barbero, T. Sokolowski, P. Kosma, H. Brade, L. Brade, T. Peters, *Biochemistry* **1999**, *38*, 6449 – 6459, and references therein.
[39] R. E. London, D. E. Pearlman, D. G. Davis, *J. Magn. Reson.* **1992**, *97*, 79 – 98.
[40] S. R. Arepalli, C. P. J. Glaudemans, G. D. Daves, Jr., P. Kovac, A. Bax, *J. Magn. Reson. Ser.B* **1995**, *106*, 195 – 198.
[41] J. L. Asensio, J. Cañada, J. Jimenez-Barbero, *Eur. J. Biochem.* **1995**, *233*, 618 – 630.
[42] F. Mohamadi, N. G. J. Richards, W. C. Guida, R. Liskamp, M. Lipton, C. Caufield, G. Chang, T. Hendrickson, W. C. Still, *J. Comp. Chem.* **1990**, *11*, 440 – 467.
[43] W. C. Still, A. Tempzyk, R. Hawley, T. Hendrickson, *J. Am. Chem. Soc.* **1990**, *112*, 6127 – 6129.
[44] T. K. Sixma, S. E. Pronk, K. H. Kalk, B. A. M. van Zanten, A. M. Berghuis, W. G. J. Hol, *Nature* **1992**, *355*, 561 – 564.
[45] InsightII (98.0), Molecular Simulations Inc., San Diego, CA, **1998**.
[46] Autodock 2.43, Oxford Molecular Ltd, Oxford, UK.
[47] 14 GRID version 17, Molecular Discovery Ltd, West Way House, Elms Parade, Oxford, UK, **1998**.

Received: March 14, 2002 [F3956]

 © 2002 WILEY-VCH Verlag GmbH & Co. KGaA, Weinheim 0947-6539/02/0820-4612 $ 20.00+.50/0